Safe and Cost-Effective Reduction of Load Postings for South Carolina Bridges

FINAL REPORT

Prepared by:

Dr. Paul Ziehl

Professor, Departments of Mechanical, Civil and Environmental Engineering

University of South Carolina

Dr. Tommy Cousins

Professor, Department of Civil Engineering

Clemson University

Dr. Brandon Ross

Associate Professor, Department of Civil Engineering

Clemson University

Dr. Nathan Huynh

Professor, Department of Civil and Environmental Engineering

University of South Carolina

FHWA-SC-23-02

January 2023

Sponsoring Agencies:

South Carolina Department of Transportation
Office of Materials and Research
1406 Shop Road
Columbia, SC 29201

Federal Highway Administration
South Carolina Division
Strom Thurmond Federal Building
1835 Assembly Street, Suite 1270
Columbia, SC 29201

Technical Report Documentation Page

1. Report No FHWA-SC-23-02	2. Government Accession No.	3. Recipient's Catalog No.
4. Title and Subtitle *Safe and Cost-Effective Reduction of Load Postings for South Carolina Bridges*		5. Report Date *January 2023* 6. Performing Organization Code
7. Author/s *Drs. Paul Ziehl, Tommy Cousins, Brandon Ross, Nathan Huynh*		8. Performing Organization Report No.
9. Performing Organization Name and Address *University of South Carolina* *Dept. of Civil and Environmental Engineering* *300 Main Street, Columbia, SC 29208*		10. Work Unit No. (TRAIS) 11. Contract or Grant No. SPR No. 752
12. Sponsoring Organization Name and Address South Carolina Department of Transportation Office of Materials and Research 1406 Shop Road Columbia, SC 29201		13. Type of Report and Period Covered *Final Report* 14. Sponsoring Agency Code
15. Supplementary Notes		

16. Abstract

South Carolina has over 9,000 bridges in its inventory, many of which were designed for H10 or H15 truck loads. Precast reinforced concrete flat slabs are the primary bridge type addressed. These components were chosen in consultation with SCDOT due to their prevalence in the bridge inventory and resolving associated performance issues will therefore have wide-ranging impact. The challenges associated with these components include a) original structural design loads that are lower than those used today, and b) ages approaching or exceeding expected lifespan in combination with deterioration. This report focuses on cost-effective, realistic, and innovative approaches to the challenges confronting South Carolina's bridge inventory. Several strengthening methods have been developed to increase the strength of posted bridges and to provide an additional target service life of 10 years.

Different strengthening approaches have been implemented on the top and bottom of the slabs, and laboratory testing has been conducted to evaluate the capacity of pre- and post-repair slabs. A cost evaluation of the implemented repair schemes is also presented. The next step in the development of strengthening approaches is field implementation.

Through field investigations followed by implementation, the approaches described are expected to minimize the number of bridge load postings. The work described is part of a larger effort to safely extend the useful life of bridges in South Carolina.

17. Key Words	18. Distribution Statement		
Bridge evaluation; precast reinforced flat slab; strengthening	No restrictions. This document is available to the public through the National Technical Information Service, Springfield, VA 22161.		
19. Security Classification (of this report) Unclassified	20. Security Classification (of this page) Unclassified	21. No. Of Pages 68	22. Price None.

Form DOT F 1700.7 (8-72) Reproduction of form and completed page is authorized.

DISCLAIMER

The contents of this report reflect the views of the authors who are responsible for the facts and the accuracy of the data presented herein. The contents do not necessarily reflect the official views or policies of the South Carolina Department of Transportation or the Federal Highway Administration. This report does not constitute a standard, specification, or regulation.

The State of South Carolina and the United States Government do not endorse products or manufacturers. Trade or manufacturer's names appear herein solely because they are considered essential to the object of this report.

ACKNOWLEDGMENTS

The authors wish to acknowledge the Steering Committee, particularly the timely and helpful input of Mark Hunter (Chair), Rodrick Tucker, Sean Futch, and Blake Gerken (FHWA), as well as Merrill Zwanka, Terry Swygert, Meredith Heaps, and Judy Hundley.

We would also like to acknowledge the support of Will Munnerlyn, who was instrumental in the execution of the project, and Russell Inglett and the technical staff at the University of South Carolina Structures and Materials Laboratory. In addition, Danny Metz, and Scott Black (technical staff for Clemson University's Built Environment Laboratory) played a critical part in the structural testing portion of this project.

The report was written with substantial input from the following:

Alex Henderson
ElHussien Elbatanouny
Laxman K C
Alyssa Leamon
Mahmoud Bayat
Li Ai

EXECUTIVE SUMMARY

Cost-effective strategies to improve the performance of precast reinforced concrete flat slab superstructures are addressed. These components are common in the SCDOT bridge inventory; therefore, addressing performance issues will have a broad impact. Challenges include a) original structural design loads that are lower than used today, and b) ages that are approaching or exceeding expected lifespan along with associated deterioration. The work described is part of a larger effort to extend the useful life of bridges in South Carolina.

The baseline behavior of precast reinforced concrete flat slabs extracted from de-commissioned bridges was experimentally established. A total of twenty slabs were tested. Twelve different flat slab tests were conducted to evaluate the existing moment capacity of the original slabs which provided a baseline behavior of these slabs. Eight more slabs were strengthened and tested to failure. The moment-displacement response of the baseline flat slab was typical of an under-reinforced concrete member, and moment capacity corresponded with the crushing of the concrete compression face.

Strengthening strategies to increase moment capacity were investigated. After a state-of-practice review, four strategies were implemented in the laboratory as proof-of-concept tests. The four strategies selected for further study were: a) attachment of steel sections to the top of the bridge deck: accomplished by either attaching two C10 x 15.3 channels to the top, or by attaching two 0.5 in. x 16 in. steel plates to the top, b) attachment of steel plates to the bottom of the bridge deck: strengthening from below was achieved by attaching plates on the bottom of the slab using four variations of plate size and attachment schemes, c) external post-tensioning attached to the deck bottom: strengthening by external post-tensioning was achieved by suspending and prestressing three 5/8 in. diameter DYWIDAG thread bars between two steel angle sections attached to the bottom of the slab, and d) near-surface mounted bars (NSM): #6 bars were embedded into the surface of two slabs in series to create one continuous slab with two spans. The advantages and disadvantages of each strategy are as follows:

a) Steel sections attached to the top of bridge deck.

   Advantage: Access is relatively easy and does not require manipulation of the underside of the bridge, existing steel reinforcement locations can be neglected.

   Disadvantages: Requires traffic control during installation; requires partial removal and replacement of the asphalt overlay (if any).

b) Steel plates attached to bottom of bridge deck.

   Advantages: Traffic control requirements are reduced; larger moment capacity increase can be achieved.

   Disadvantages: Requires access from the underside of the bridge deck; requires partial removal and replacement of asphalt overlay (if any) for the case of through bolting; steel exposed to the elements and susceptible to corrosion; significant ductility decrease compared to all other tests.

c) External post tensioning attached to the deck bottom.

   Advantages: Larger moment capacity increase can be achieved, self-weight of the

strengthening system is not high

Disadvantages: Threadbars which are applied externally are vulnerable to corrosion; requires access from the underside of the bridge deck; requires partial removal and replacement of asphalt overlay (if any) for the case of through bolting.

d) Near-surface mounted (NSM) bars

Advantages: Access is easy and does not require manipulation of the underside of the bridge; existing steel reinforcement locations can be neglected.

Disadvantages: Requires traffic control during installation; requires partial removal and replacement of the asphalt overlay (if any).

Strengthening from the bottom with a steel plate increases the flexural strength up to 41% (Method 2,12 holes). The total moment increase for the strengthened slab with steel channels from above was 12%. The slab with steel plates from above increased the moment capacity by 4%. The slab with external post tensioning increased the moment capacity by 42%. The slab with near surface mounted bars increased the applied load capacity by 23%. All increases in capacity were compared to the average of the baseline (unstrengthened) specimens.

TABLE OF CONTENTS

LIST OF FIGURES

LIST OF TABLES

CHAPTER 1: INTRODUCTION

1.1 Description of problem

South Carolina has more than 9,000 bridges in its inventory, many of which were designed for truck loads that are less than current standards. To proactively address this situation, the South Carolina Department of Transportation (SCDOT) has recently engaged engineering consultants to load rate the bridge inventory of the state. The load rating effort is expected to provide meaningful information on the current inventory condition. However, it is not expected to result in detailed recommendations for repair, rehabilitation, or replacement options. The load rating effort and its findings are focused on diagnosing issues and identifying posting requirements, but not prescribing restoration treatments. This report presents cost-effective, realistic, and innovative approaches tailored to the technical challenges facing the bridge inventory of South Carolina.

In this report, one specific challenge is addressed: precast reinforced concrete flat slab superstructures. This component was selected through consultation with SCDOT due to its prevalence in the bridge inventory; therefore, addressing performance issues for precast flat slabs will have a broad impact. Challenges associated with these bridges include a) original structural design based on lower truck loads than currently used, and b) exceedance of expected lifespan and associated deterioration - thereby impacting load capacity and durability. These challenges represent direct costs due to bridge upgrades and replacements and indirect costs due to the re-routing of trucks, increased travel time for emergency routes, and construction delays for motorists. The results are expected to mitigate these issues with cost-effective approaches for reducing the number of bridge postings.

Furthermore, the inspection of the bridges is needed to identify the present conditions of the bridge. The presence of defects that could degrade the performance of the bridge should be identified in the early phase to avoid bigger structural damage in the future. Manual visual inspections are carried out in the field which is challenging and costly. The report presents an automated method of inspection of the bridges which is safe and cost-effective.

1.2 Background

Many of the bridges on South Carolina's secondary routes were designed using either H-10 or H-15 load criteria. These are two-axle design trucks having a total weight of ten tons (20 kips) for H-10 and 15 tons (30 kips) for H-15. Based on the data from SCDOT, there are 3,622 bridges in South Carolina that were designed using H-10 or H-15 criteria. This is approximately 39% of the state inventory. Due to the widespread challenges with H-10 and H-15 bridges, the development of cost-effective, realistic, and innovative retrofit methods will result in significant direct and indirect savings for the state of South Carolina.

H-10 and H-15 truck loads are significantly less than the current HL-93 design truck (AASHTO 2017). Consequently, the H-10 and H-15 bridges have less live load capacity and in general, cannot support the loads carried by newly designed and built bridges. The age and condition of H-10 and H-15 bridges are also of interest as many of these bridges have experienced deterioration associated with decades of service. The ongoing task of load rating South Carolina's bridges will result in recommendations to post, retrofit, or replace numerous H-10 and H-15 bridges.

1.3 Objectives

The investigations addressed in this report are part of a multi-year research investigation. The overarching goal is to identify and develop cost-effective analysis and strengthening strategies, thereby leading to a reduction of load postings. As an outcome, the useful life of bridges in South Carolina will be extended.

Specific goals of the project include:

- Benchmarking the flexural strength of precast concrete flat slabs.
- Evaluating a flat slab strengthening methods using steel channels or steel plates bolted to the top of the slab.
- Evaluating a flat slab strengthening method using steel plates bolted to the bottom of the slab.
- Evaluating a flat slab strengthening method by external post tensioning at the bottom of the slab
- Evaluating a flat slab strengthening method by near-surface-mounted technique.
- Evaluating traditional and numerical models of flat slabs.
- Benefit cost analysis of the different strengthening approaches

These goals are addressed through experimental, analytical, and computational methods.

CHAPTER 2: LITERATURE REVIEW

2.1 Overview of slab strengthening

Petrou et al. (2008) examined a retrofit scheme for strengthening reinforced concrete (RC) bridge decks composed of attaching carbon fiber reinforced polymer (CFRP) to the soffit of the slabs. One-way and two-way reinforced concrete slabs strengthened with CFRP were investigated under the effect of monotonic and cyclic loading to failure.

Five one-way reinforced concrete slabs were taken from a utility bridge in Charleston, SC. The slabs were 8.5 in. thick, 60 in. wide, and 14 ft long. The slabs were longitudinally reinforced by ten No. 7 reinforcing bars with 6 in. spacing and No. 4 reinforcing bars at 12 in. spacing in the transverse direction. The slabs were retrofitted using six 1.33 in. wide strips of CFRP attached to the soffit with the spacing of 10 in. on center. Figure 2.1 presents the typical details of the slabs and the retrofit system. The specimen designation and the material properties for one-way slabs are presented in Table 2.1.

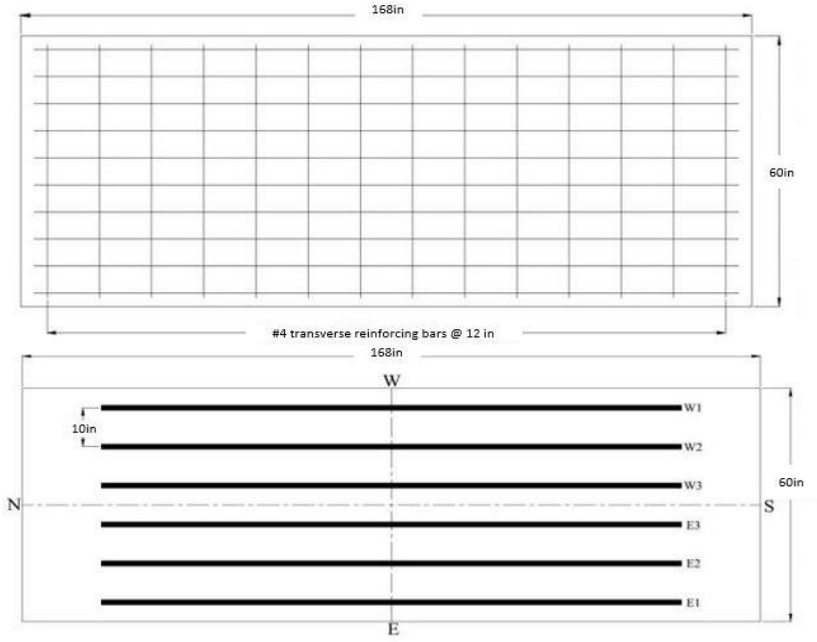

Figure 2.1 Specimen and retrofit details for the one-way slab, (Petrou et al., 2008).

Table 2.1 One-way slab specimen designation and material properties (Petrou et al., 2008)

Specimen	Unretrofit (U)	Retrofit (R)	Monotonic testing (M)	Fatigue testing (F)	Concrete strength (psi)	Reinforcing steel strength, f_y, (ksi)
1UM	X		X		5200	60
1RM1		X	X		5200	60
1RM2		X	X		5200	60
1UF	X			X	5200	60
1RF		X		X	5200	60

*1 refers to one-way slabs

Six half-scale two-way reinforced concrete slabs were cast and constructed as square slabs based on a prototype design of a highway bridge deck. The slabs were 52 in. long and 3.75 in. thick. The slab reinforcement comprised both top and bottom layers of D5 wire reinforcement in the longitudinal and transverse directions. At the bottom layer, the D5 wire reinforcement was spaced at 4 in. on center in both directions. For the top layer, the spacing was 6 in. on center in both directions. Figure 2.2 presents specimen cross-section details. Grid and strip retrofit were the two different techniques to strengthen the two-way slabs. The CFRP was attached to the soffit of the slabs in both directions for the grid retrofit; the strip retrofit was only attached in the longitudinal direction. The specimen designation and material properties for the two-way slabs are presented in Table 2.2.

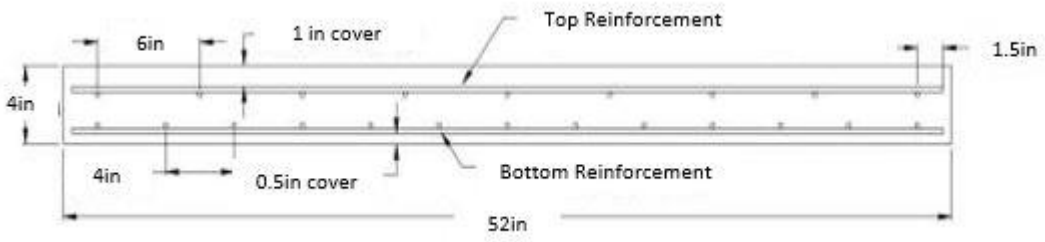

Figure 2.2 Half-scale two-way slab specimen details (Petrou et al., 2008).

Table 2.2 Two-way slab specimen designation and material properties (Petrou et al., 2008)

Specimen	Unretrofit (U)	Strip retrofit (S)	Grid retrofit (G)	Monotonic testing (M)	Fatigue testing (F)	Concrete strength (psi)	Reinforcing steel strength f_y, (ksi)
2UM	X			X		3464	80
2SM		X		X		3464	80
2GM			X	X		3464	80
2UF	X				X	3464	80
2SF		X			X	3464	80
2GF			X		X	3464	80

*2 refers to two-way slabs

The slabs were simply supported for both monotonic and cyclic (fatigue) loading. The load-deflection curves for the monotonic specimens are shown in Figure 2.3, showing that all retrofitted slabs have higher ultimate strength than the unretrofit control specimens. For monotonically loaded one-way slabs, 1RM1 and 1RM2 had 14.8% and 18.1% higher ultimate strength, respectively, over the control specimen 1UM. On the other hand, for monotonically loaded two-way slabs, 2SM and 2GM had 13.8% and 10.7% higher ultimate strength, respectively, over the control specimen 2UM. The cyclically loaded one-way slab specimens were subjected to three different peak load cycles of 27, 38, and 51 kips. In comparison, the two-way slab specimens were subjected to two cycles of 7.5 and 26 kips. The retrofit specimen 1RF endured 60% more cycles at 51 kips peak load than the unretrofit control specimen 1UF. Also, the retrofit specimens 2SF and 2GF endured 43.6% and 287%, respectively, at 26 kips peak load than the unretrofit control specimen 2UF.

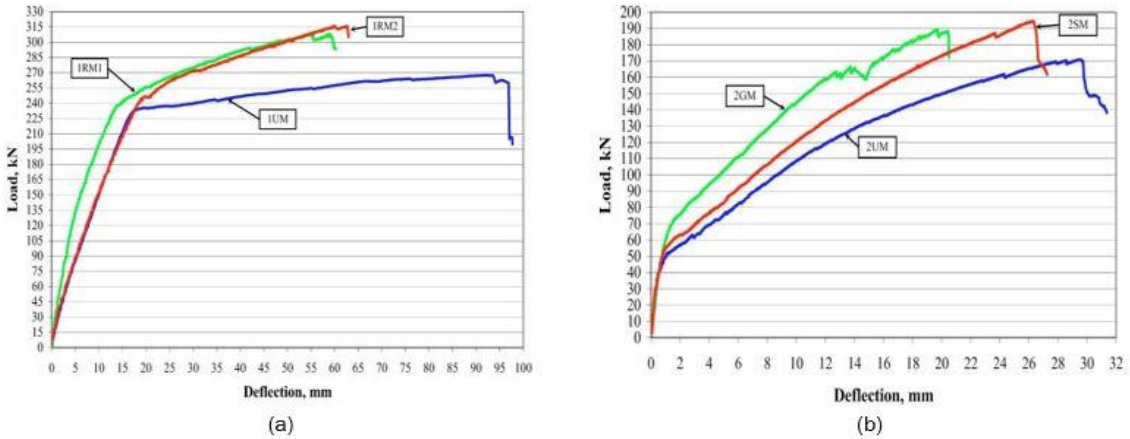

Figure 2.3 Monotonic load-deflection behavior (a) one-way slab specimens (b) two-way slab specimens (Petrou et al., 2008).

Yuan et al. (2020) proposed a method to strengthen reinforced concrete members with high-strength steel wire covered by high ductile engineered cementitious composites (ECC). Nine reinforced concrete beams were tested. The length of the beams was approximately 5.9 ft with a width of 5.9 in., and 10 in. thickness. One beam was a control specimen without strengthening, while the other eight beams were strengthened with high-strength steel wires covered by either polymer mortar or ECC. The steel wires were attached to the reinforced concrete (RC) beams, as shown in Figure 2.4. The reinforcement of the beams was the same, and it was calculated on the basis that the beams would fail in flexure. The parameters that varied were the matrix type for the strengthened layer, the number of wires, and the existence damage of the specimens. The specimen designation is shown in Table 2.3, where RC refers to the control specimen while SSP and SSE refer to the strengthened specimens with steel wires alongside polymer mortar and ECC as the matrix type, respectively.

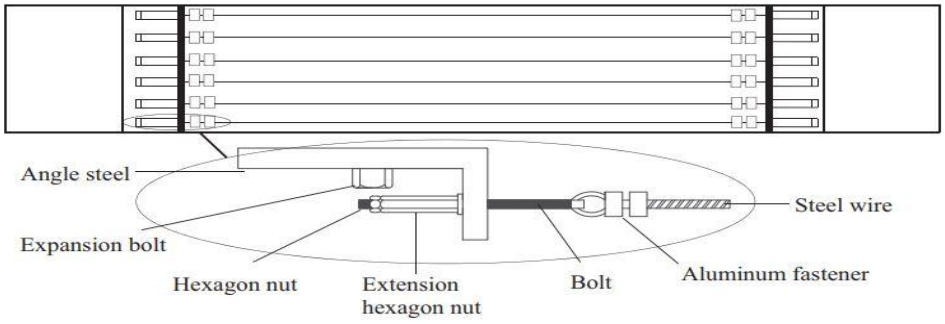

Figure 2.4 Details of developed steel wires and strengthening procedure (Yuan et al., 2020).

Table 2.3 Specimen Designation (Yuan et al., 2020)

Specimen	No. of Steel wire	Mortar type	pre-damage	Strengthened with steel wire
RC-0	-	-	No	No
SSP-2	2	Polymer mortar	No	Yes
SSP-4	4	Polymer mortar	No	Yes
SSP-6	6	Polymer mortar	No	Yes
SSE-2	2	ECC	No	Yes
SSE-4	4	ECC	No	Yes
SSE-6	6	ECC	No	Yes
SSP-6P	6	Polymer mortar	Yes	Yes
SSE-6P	6	ECC	Yes	Yes

A four-point bending test was conducted on the beams. The moment versus deflection curves at midspan for the beams are shown in Figure 2.5. All strengthened specimens showed higher cracking strength, yield strength, and ultimate strength than the unstrengthened specimen. The results revealed that the increase in strength accompanies the increase in the number of wires. Moreover, SSE strengthened specimens have greater improvement in strength than the SSP strengthened specimens, as presented in Table 2.4. The maximum increase in the ultimate strength was 66.5% for the SSE-6P specimen compared to the control specimen.

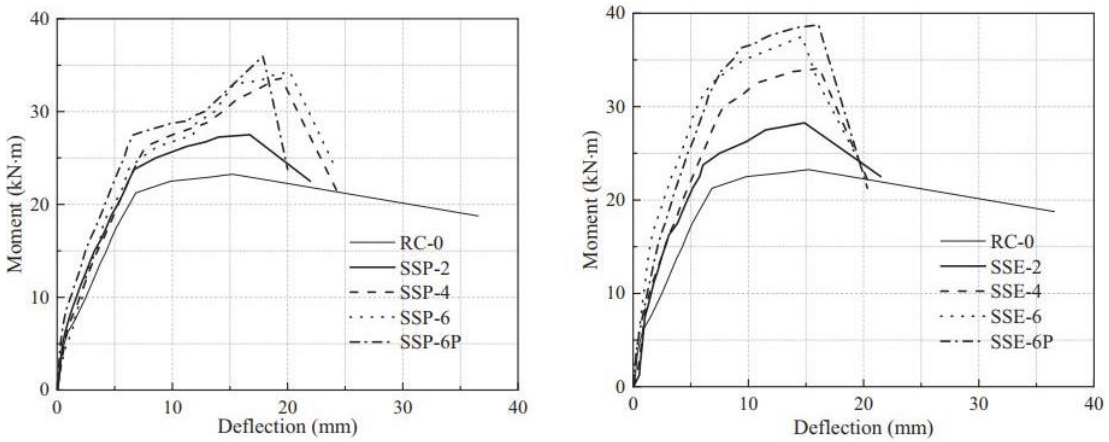

Figure 2.5 Moment versus mid-span deflection curves of the specimens (Yuan et al., 2020).

Table 2.4 Strength Indexes of the beam specimens (Yuan et al., 2020)

Specimen	Cracking moment (kip-ft)	Yielding moment (kip-ft)	Ultimate moment (kip-ft)	Cracking moment improvement (%)	Yielding moment improvement (%)	Ultimate moment improvement (%)
RC-0	3.8	12.0	17.2	NA	NA	NA
SSP-2	4.6	13.9	20.3	23.5	15.3	18.0
SSP-4	6.1	16.6	24.9	62.7	38.0	45.1
SSP-6	6.1	19.2	25.4	62.7	60.1	47.6
SSE-2	7.9	14.7	20.9	109.8	22.7	21.5
SSE-4	7.6	17.3	25.2	102.0	43.6	46.8
SSE-6	6.5	19.4	27.6	72.5	61.3	60.9
SSP-6P	-	18.4	26.5	-	53.4	54.5
SSE-6P	-	21.2	28.6	-	76.7	66.5

*NA refers to not applicable

Wibowo and Sritharan (2018) studied the flexural behavior of slabs reinforced with ultra-high-performance concrete (UHPC) on the top and bottom of the slab. Three simply supported specimens with dimensions of 2 ft. x 8 ft. and span of 6 ft., were constructed to represent the concrete slab of a bridge deck in Iowa and tested in the lab. A concrete diamond saw was used to manually groove the surface to the required roughness. Wire mesh was placed on top of the roughened surface to emulate the condition of the Mud Creek bridge. The concrete surface was dampened to reduce the loss of water due to absorption. One layer of 1.5 in. thick UHPC was placed on the top of two slabs whereas one slab had no concrete overlay (referred to as NO). The compressive strength of the concrete used in the actual slabs was 6.6 ksi, whereas the strength of the UHPC overlay was eighteen ksi. The concrete overlay was kept on top of one of the slabs named OT to investigate the positive moment behavior. The other slab was kept upside down, with the bottom side having the concrete overlay (referred to as OB) to investigate the negative moment behavior.

The mode of failure for specimen NO (no UHPC overlay) was shear. A large shear crack formed near the support at the failure. Specimen OT (with UHPC on top) failed at a larger load also in shear. The shear crack propagated to the UHPC layer and separated the UHPC and normal concrete layer horizontally. A single flexural crack formed in the UHPC layer in slab OB (with UHPC at the bottom) that penetrated the UHPC layer at midspan. The crack propagated to the top causing flexural tension failure and crushing of concrete at the top. The addition of the UHPC layer on the top of slab OT increased the strength and stiffness. The OT slab also showed an increase in ductility due to the presence of UHPC, which carried compressive stress on the slab. An increase in strength in slab OB was observed, which could be attributed to the increase in depth due to the overlay.

Lee et al. (2018) studied the change in flexural strength in pre-damaged beams strengthened using post-tensioned external steel rods. A total of nine beams were tested under three-point loading. Three different amounts of tension reinforcement were used in the beams while keeping the compression reinforcement and concrete strength the same. Reference beams were named S1-No, S2-No, and S3-No. Post tensioning was applied to six beams. Post tension force in the external rods was applied by manually tightening nuts at the location of anchorage. Steel rods having a diameter of 0.87 in. (22 mm) and 1.10 in. (28 mm) were used for post-tensioning each type of beam. R22 and R28 were used to represent the steel rod diameter in the name of each specimen.

Strengthened beams were named S1-R22, S1-R28, S2-R22, S2-R28, S3-R22, and S3-R28. Details of the specimen are shown in Table 2.5 and Figure 2.6 below.

Table 2.5 Description of beams (Lee et al., 2018)

No.	Specimen	A'_s (sq. in.)	$\frac{f'_y}{f'_u}$(ksi)	A_s (sq. in.)	$\frac{f_y}{f_u}$ (ksi)	A_{ps} $(sq.\ in.)$	$\frac{f_{py}}{f_{pu}}$ (ksi)	d_p	Section (in.)
1	S1-No	0.59	$\frac{78.90}{95.00}$	2.77	$\frac{72.52}{92.82}$	n/a	n/a	n/a	b=10.62
2	S1-R22					1.18	$\frac{95.00}{116.76}$	17.13	h=15.74
3	S1-R28					1.91	$\frac{90.65}{110.95}$	17.13	d=13.85
4	S2-No	0.59	$\frac{78.90}{95.00}$	1.78	$\frac{71.50}{91.37}$	n/a	n/a	n/a	b=10.62
5	S2-R22					1.18	$\frac{95.00}{116.76}$	17.13	h=15.74
6	S2-R28					1.91	$\frac{90.65}{110.95}$	17.13	d=13.85
7	S3-No	0.59	$\frac{78.90}{95.00}$	1.33	$\frac{71.50}{91.37}$	n/a	n/a	n/a	b=10.62
8	S3-R22					1.18	$\frac{95.00}{116.76}$	17.13	h=15.74
9	S3-R28					1.91	$\frac{90.65}{110.95}$	17.13	d=13.85

A'_s is the compression reinforcement f'_y and f'_u are the yield and ultimate strength of steel in compression A_s is the area of tension reinforcement f_y and f_u are the yield and ultimate strength of steel in tension A_{ps} is the area of external prestressing steel rods	f_{py} and f_{pu} are the yield and ultimate strength of prestressing steel rods d_u is the depth of steel rods at the deviator b is the width of the beam h is the height of the beam d is the effective depth of tensile reinforcement

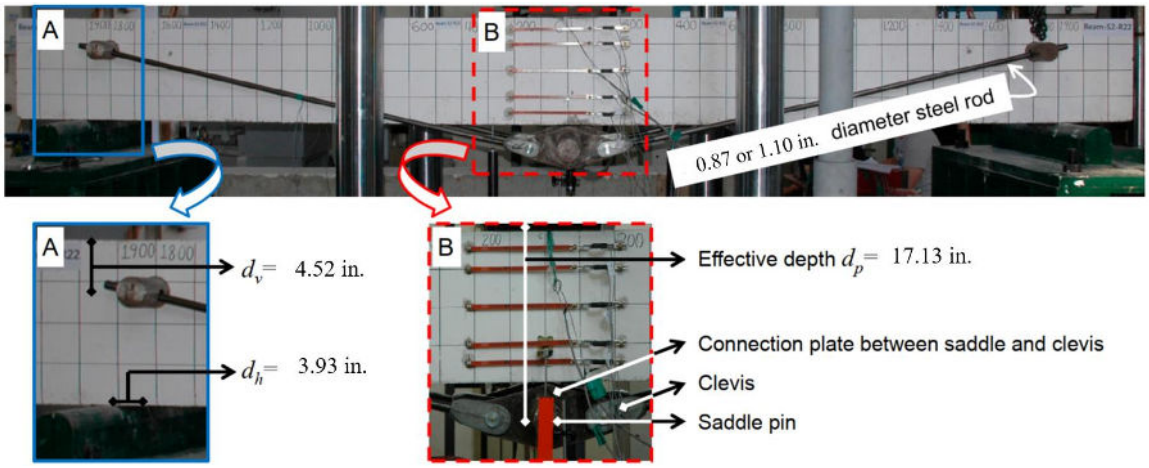

Figure 2.6 Details of beam specimen (Lee et al., 2018).

The behavior of the reference beams was summarized in three stages: initiation of cracks, yield of tensile reinforcement, and crushing of concrete to collapse. Beam specimen S1-No with the highest amount of tensile rebars showed the highest load carrying capacity of 74.4 kips. S2-No showed a load carrying capacity of 51.3 kips, and S3-No, which had the lowest number of tensile bars, showed the lowest load carrying capacity of 40.7 kips.

All beams strengthened with external post-tensioning showed fewer and less narrow cracks and an increase in yield and ultimate load in comparison to the reference beams. Load capacity of specimen type S1 increased by 40% to 105.4 kips for S1-R22 and 55% to 117.1 kips for S1-R28. An increase in load of 64% to 94.2 kips and 101% to 115.3 kips was observed in specimen types S2-R22 and S2-R28, respectively. Similarly, load capacity increased by two times to 91.9 kips and 98.2 kips for the specimen type S3-R22 and S3-R28, respectively. The beams strengthened with a thicker diameter of steel rods showed higher strength.

Gao et al. (2020) proposed a method of anchoring external post-tensioned glass fiber-reinforced polymer (GFRP) tendons to one-way slabs to improve flexural behavior. Six slabs with 19.7 in. width, 78.7 in. length, and 3.9 in. thickness in a simply supported condition were tested in four-point bending. The details of these specimens are shown in Table 2.6. Figure 2.7 shows the schematic representation of a post-tensioned slab. Two hydraulic jacks were used to apply prestressing, and a load cell was used to monitor the level of prestressing in the tendons as shown in Figure 2.8. Three externally post-tensioned GFRP tendons at prestressing of 8.7 ksi, 11.6 ksi and 14.5 ksi were used to strengthen GRC3-1, GRC3-2, and GRC3-3 specimens. Two and four tendons at prestressing of 11.6 ksi were used to strengthen GRC2-2 and GRC4-2 whereas no modification was made to the control slab (referred to as RC0).

Table 2.6 Description of the slabs (Gao et al., 2020)

Slab	Reinforcement Area (in^2)	Reinforcement Depth (in.)	Prestressing tendon area (in^2)	Prestressing tendon depth, (in.)	Prestressing level, (ksi)	Net span, (in.)
RC0	0.31	3.19	-	-	-	70.87
GRC2-2	0.31	3.19	0.16	5.12	11.60	70.87
GRC3-1	0.31	3.19	0.23	5.12	8.70	70.87
GRC3-2	0.31	3.19	0.23	5.12	11.60	70.87
GRC3-3	0.31	3.19	0.23	5.12	14.50	70.87
GRC4-2	0.31	3.19	0.31	5.12	11.60	70.87

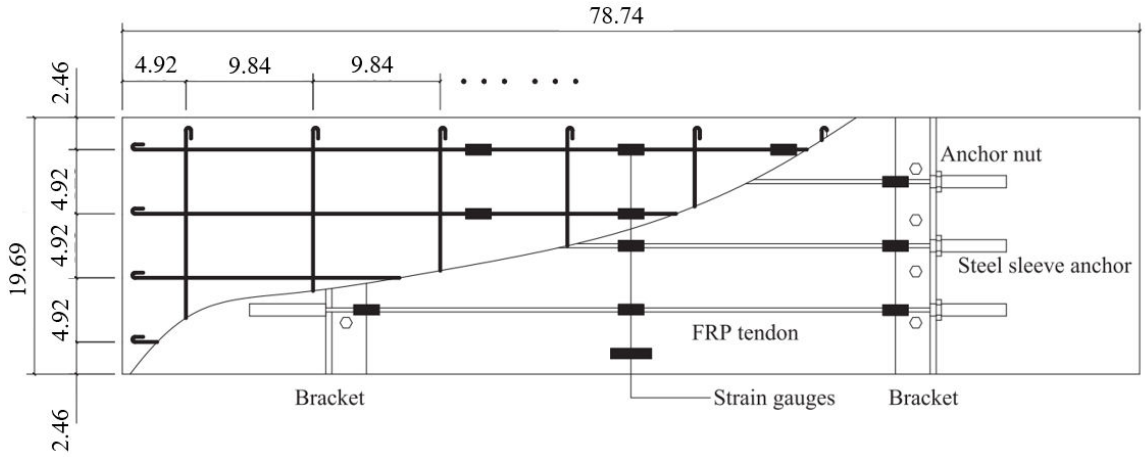

Figure 2.7 Bottom of one-way slab with three GFRP tendons (Gao et al., (2020)).

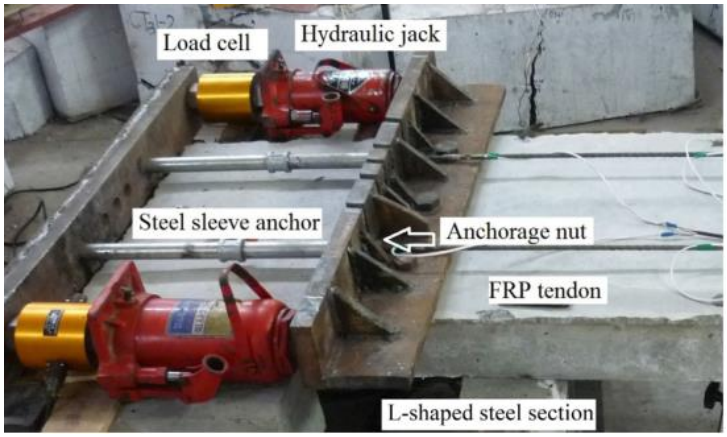

Figure 2.8 Pre-tensioning of tendons (Gao et al., 2020).

A hydraulic jack was used to apply load to failure. The results indicate that all strengthened slabs have a higher first crack moment, yield moment, and ultimate moment compared to the control specimen. Slab GRC2-2 had 24%, GRC3-1 had 42.2%, GRC3-2 had 85.8%, GRC3-3 had 51.1% and GRC4-2 had 121% higher moments at first cracking than RC0 (control specimen). Slab GRC2-2 had 8.93%, GRC3-1 had 6.92%, GRC3-2 had 74%, GRC3-3 had 39.5% and GRC4-2 had 67.9% higher moments at yield in comparison to specimen RC0. Slab GRC2-2 had 38.6%, GRC3-1 had 30.6%, GRC3-2 had 79.9%, GRC3-3 had 69.4% and GRC4-2 showed 103% higher ultimate moment than RC0. The moment deflection curve for the slabs was plotted to study the flexural behavior which is shown in Figure 2.9. The effect of strengthening was not significant in the initial stages prior to the cracking of concrete. However, the first cracking, yielding, and ultimate moment of the slabs were increased with a higher number of tendons and higher prestressing level.

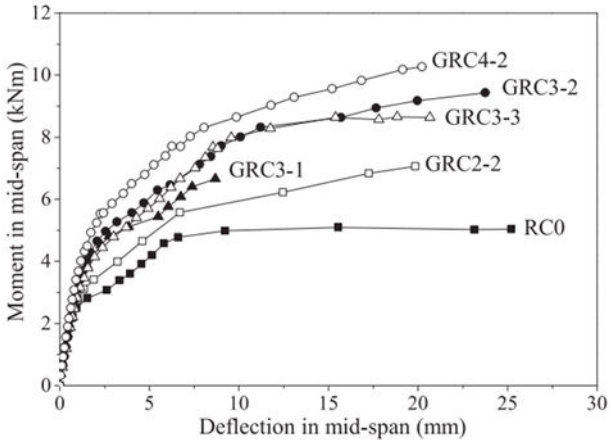

Figure 2.9 Moment deflection curves (Gao et al., 2020).

2.2 Drone based inspection for damage detection

The bridges in the inventory have been subjected to decades of service deterioration. An inspection of the bridge is required to find the critical defects that can potentially ruin the bridge's functionality. The defects such as cracks, delamination, spalling, and corrosion that can cause the reduction in critical strength of the bridge should be detected. Cracks on the surface of the structure are the early signs of distress. Delamination and spalling of concrete causes loss of the cross-section of the concrete in the bridge resulting in the reduction of load carrying capacity. Corrosion of the steel reinforcement can reduce the rebar cross-section reducing the tensile strength of the bridge. Corrosion can lead to the degradation of the bond between the concrete and the steel reinforcement which could be detrimental to the bridge’s performance. Countermeasures may be suggested after evaluating these defects and assessing the structural integrity of the bridge (Kim et al., 2017).

Inspection of the bridges is accomplished through manual visual inspection of concrete surface. The bridge on the site is inspected visually for the presence of defects. However, this may be costly, labor intensive, and pose risks to the safety of inspectors. The assessment of the condition of the bridge is also subjected to the skills and experience of the personnel inspecting the bridge. To eliminate these limitations, automated inspection of the bridge is proposed in the study. With the advances in Unmanned aerial vehicles (UAV) technology, the UAVs have been utilized in the

construction of three-dimensional models for bridge safety inspection, condition evaluation, and surveillance of traffic flow (Lei et al., 2018). UAVs are used to carry the camera and transmit images to be stored for post-processing to monitor the deterioration of bridges. The use of drones helps in reducing the budget, reducing the risk of work accidents, and will not interfere with traffic compared to the traditional method of inspection (Metni and Hamel, 2007). With the development of techniques for image processing, sensors, and automated inspection methods are increasingly used to identify the presence of defects. The severity of the defects on the bridges is assessed automatically by the method objective.

Different methods of image processing have been applied to effectively extract information of cracks from images of the bridge surfaces. Abdel-Qader et al. (2003) implemented various techniques to automatically detect cracks and to assess deterioration in the bridge. Four algorithms for edge detection, Sobel, Canny, fast Fourier transform (FFT), and fast Haar transform (FHT), were analyzed in MATLAB and their effectiveness was compared. Fifty images of the bridge surfaces with and without cracks were read and transformed using these algorithms to get an output of isolated cracks. The resulting images from FHT eliminated noise produced by concrete patterns and produced highly accurate representations of cracks in the images. The presence of cracks in the images was determined by a threshold value calculated using an average of the intensity of pixels in the crack images. Results showed a combined accuracy of 86% using the FHT technique, 76% using Canny, 68% using Sobel, and 64% using the FFT technique for the detection of cracks.

With the development of image processing techniques and computer vision methods, neural networks and deep learning have been used to process the images and assess the condition of the bridges. Moon and Kim (2011) proposed an automatic crack detection system that can analyze the concrete surface and visualize the cracks efficiently using neural networks. In the first step, cracks are distinguished from background images using filtering, the improved subtraction method, and morphological operation. In the second step, the existence of cracks is identified. A backpropagation neural network is used to automate image classification. A backpropagation neural network was trained using 105 images of concrete structures, and the trained network was tested for 120 new images. The recognition rate of the crack image was 90%, and the non-crack image was 92%. This method is useful for non-expert inspectors enabling them to perform crack monitoring tasks effectively. A deep learning method was implemented by Cha et al. (2017) to effectively detect the presence of cracks in concrete images. A convolutional neural network (CNN) was implemented to train and test 332 images under different lighting conditions. An accuracy of 98.2% in training and an accuracy of 98.0% in validation for the detection of cracks were recorded using this method. Low noise levels and robust performance in varying lighting conditions were observed using the deep learning approach. Clear and accurate crack information was produced as shown in Figure 2.10 using the CNN algorithm.

a. Original image b. Image from CNN method

Figure 2.10 Crack detection utilizing CNN (Cha et al., 2017).

A deep learning CNN model was implemented by Savino and Tondolo (2021) for automatic classification of damages in the concrete. Images of the concrete surfaces collected from the internet were fed to the CNN model for training and testing. A GoogLeNet model was selected which had the validation accuracy of 94% in classifying these images. Transfer learning method was used to classify the images of the concrete surface as "undamaged," "cracked," and "delaminated" based on their respective conditions. The proposed model was checked for reliability in classifying the images collected from the real bridge structures, tunnels, and pavements. The model was found to be effective in inspecting the images. Zhu and Song (2020) proposed an improved visual geometry group network-16 (VGG-16), for the classification of the defects in the surface of the concrete bridges. The model was efficient and robust in detecting the defects in the images with an accuracy of 99%. Zhu et al. (2020) developed a vision-based method to detect defects by implementing a CNN model. A large dataset of images collected from the internet was split into five different classes namely: intact, crack, pockmark, spalling, and exposed rebar. The inception-v3 module was developed to analyze large numbers of images and automatically identify the defects. The model trained on the image dataset was tested on 134 images from bridges in various locations. An accuracy of 97.8% was recorded for the testing data which was not used in the training phase.

Kim et al. (2017) used the method of hybrid image processing using images from a UAV to identify cracks and extract information about the width and length. One set of binarization parameters was applied to the images to calculate the width of the crack, and the second set was applied to calculate the length of the crack. After binarization of the images crack segments were represented by black pixels connected in each group. The crack segment was differentiated as a skeleton; pixels in the center, and edges; and pixel group at the outer part, as shown in Figure 2.11. The skeleton is analyzed to obtain the length of the crack and information about the direction of the crack. The distance from the two edge pixels to the nearest skeleton pixel is used to obtain the width of the crack. The hybrid method was found to be dependable in measuring the width of the cracks having thickness of more than 0.1 mm and estimating the length of the crack with an error of 7.4%.

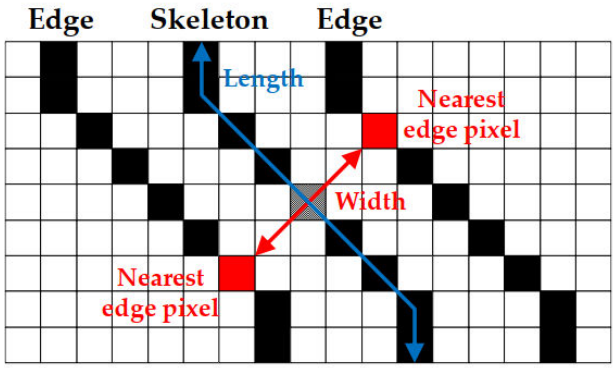

Figure 2.11 Illustration of width and length of the crack (Kim et al., 2017).

Zhu et al. (2011) implemented modifications in the percolation-based method of image processing for mapping cracks. An image thinning technique and distance transform were used to retrieve the properties of the crack. The distance field and information related to the segment of the crack skeleton were used to extract the length of the crack, which is the same as the length of the segment of the crack skeleton, which is the height of the bounding box circumscribing the points of the segment of the crack skeleton. The orientation of the crack is denoted by the orientation of the same box. The double average distance from the skeleton to the nearest edge indicated the width of the crack. The largest value of distance existing on the skeleton is doubled to get the maximum width of the crack and the shortest value existing when doubled represents the minimum width of the crack. The spatial correlation was used between the image pixel value and the orientation and dimension of structural elements to obtain the relative measurements. An error of 3.29 degrees, 2.21%, and 0.35% were observed for the crack property orientation, crack length, and maximum width of the cracks measured, respectively.

Automatic detection of the defects and quantification of the defects can help in the inspection to arrive at a decision regarding further assessment and the need for countermeasures to extend the functionality of the bridge. Several methods have been proposed in the literature to identify and quantify the presence of defects in the structure. The report will present the development of an accurate CNN model, a type of deep learning technique, for the inspection of presence of cracks in the precast slab bridges. Secondly, a multiclass CNN model will be presented which can classify the images containing cracks to different damage zones based on the depth of the crack.

CHAPTER 3: METHODOLOGY

The overarching goal is to identify and develop cost-effective strengthening strategies that can lead to an increase in load ratings. This chapter addresses several strengthening approaches and laboratory investigations for precast reinforced concrete flat slabs.

3.1 Flat slab test setup

Flexural tests of precast reinforced concrete flat slabs, commonly used in older short-span bridges in South Carolina, were conducted at the University of South Carolina (USC) and Clemson University (CU). The flexural tests investigated both baseline performance and performance of strengthened slabs. The slab specimens tested were originally used in a SCDOT bridge, for at least three decades, and were stored in a SCDOT facility. Dimensions of the slabs are 8.25 in. thick, 5 (or 5.5) feet wide, and 14 (or 15) feet in length. Based on SCDOT drawings, typical bottom reinforcement for precast reinforced concrete flat slabs is No. 7 bars @ 6 in. on center longitudinally, No. 4 @ 12 in. on center transversely (Figure 3.1), and the specified compressive strength of the concrete was $f_c' = 4000$ psi***. Based on the drawings and the age of the slabs, it was assumed that the*** **yield strength of the reinforcing steel** ***was*** $f_y = 40000$ psi***. Specimens of both concrete and steel rebar were taken from the slabs to be tested, and the results are shown in Table 3.1 and***

Table 3.2, respectively. A total of twenty tests were completed: 12 baseline tests (four with 14 ft. span length and eight with a 15 ft. span length), two tests on slabs strengthened with steel channels/plates on top, four tests on slabs strengthened from the bottom, one with external post tensioning, and one with near surface mounted (NSM) bars.

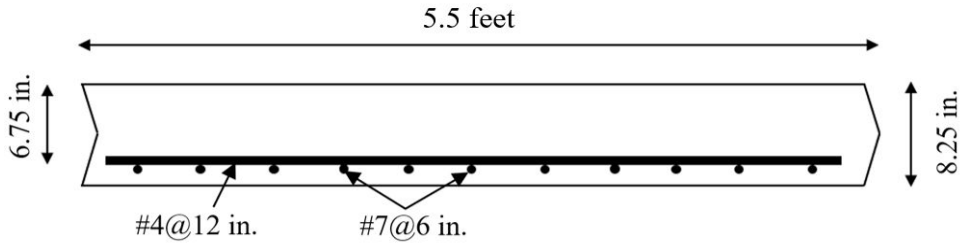

Figure 3.1 Dimensional information and reinforcing details of 15-foot flat slab specimens.

Table 3.1 Precast concrete slab compressive strength from cores tested per ASTM C 109

	Strength (psi) **(WSP)**	Strength (psi) **(USC)**
Number of cores	99	43
Average Tested	6890	7401
Minimum Tested	3990	3960
Maximum Tested	10350	11120
Specified	4000	4000

Table 3.2 Tensile strength of 6 rebar specimens in precast concrete slabs tested per ASTM E8

	Yield Stress (ksi)	Ultimate Stress (ksi)
Average Tested	49.1	77.6
Minimum Tested	46.5	74.0
Maximum Tested	56.0	92.5
Specified	40.0	55.0

3.1.1 Baseline slabs

Figure 3.2 shows schematics of the test setup used at both USC and CU. The details of the test setup (including span length (L) and slab width (E)) are presented in Table 3.3. All tests had neoprene bearing pads supporting the slabs at each end except test No.4, which had pin and roller supports at each end. Figure 3.3 shows photographs of tests in progress at USC and CU.

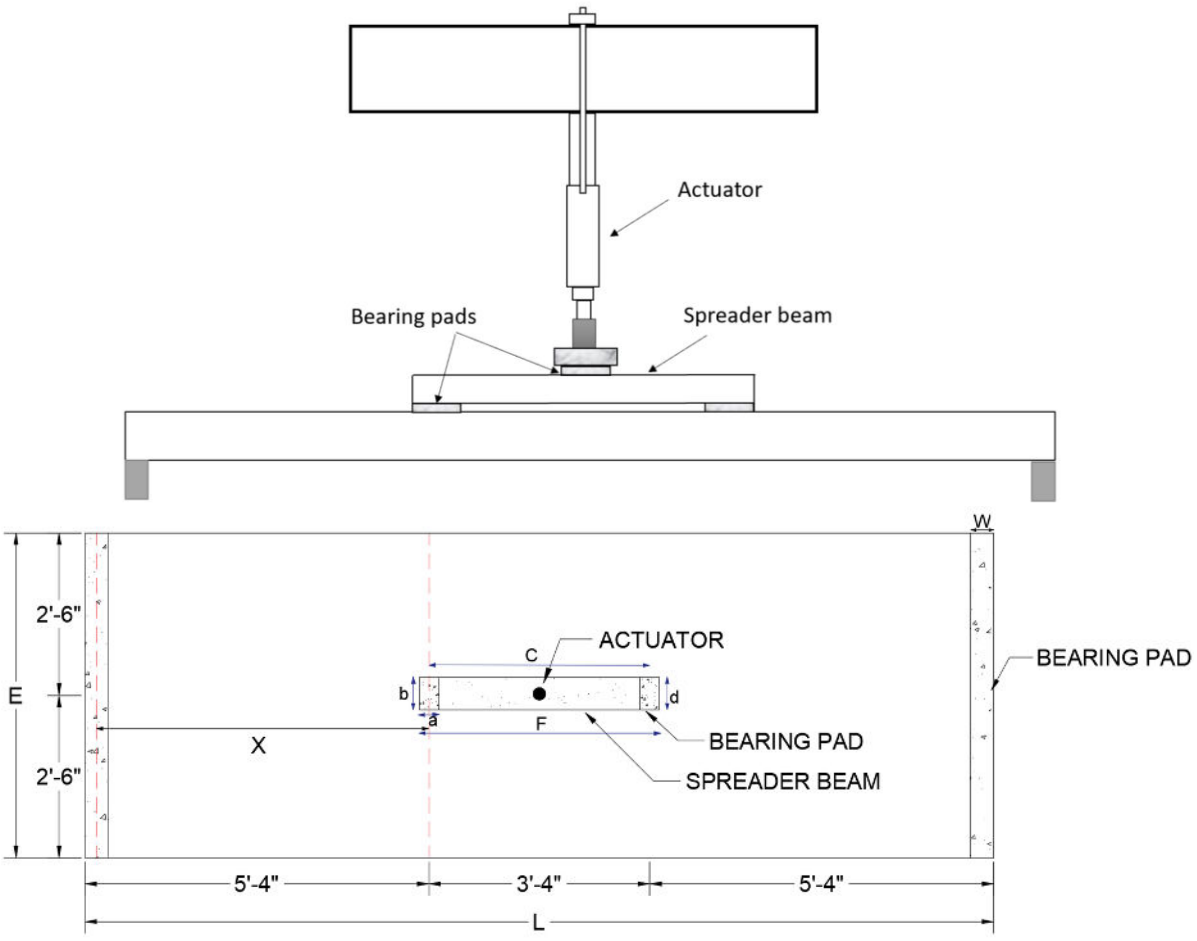

Figure 3.2 Elevation (top) and plan view (bottom) of flat slab test setup.

Table 3.3 Description of test specimens

Test	University	L	E (Width)	D	Support condition	W	a	b	A (a*b)	c	d	F	X
1	CU	14	5	8.25	Bearing	9	8	8.5	68	40	8.5	52.0	4.95
2	CU	14	5	8.25	Bearing	9	8	8.5	68	40	8.5	52.0	4.95
3	CU	14	5	8.25	Bearing	9	8	8.5	68	40	8.5	52.0	4.95
4	CU	15	5.5	8.25	Roller	N/A	8	8.5	68	40	8.5	52.0	5.45
5	CU	15	5.5	8.25	Bearing	9	8	8.5	68	40	8.5	52.0	5.45
6	USC	15	5.5	8.25	Bearing	9.5	8.5	8.5	72.25	40	8.5	51.7	5.43
7*	USC	14	5	8.25	Bearing	9.5	8.5	8.5	72.25	40	8.5	51.7	4.95
8*	USC	14	5	8.25	Bearing	9.5	8.5	8.5	72.25	40	8.5	51.7	4.95
9*	CU	14	5	8.25	Bearing	9	8	8	64	40	8	52	4.95
10	USC	14	5	8.25	Bearing	9	8	8.5	68	40	8.5	52.0	4.95
11	USC	15	5.5	8.25	Bearing	9.5	8.5	8.5	72.25	40	8.5	51.7	5.43
12	USC	15	5.5	8.25	Bearing	9.5	8.5	8.5	72.25	40	8.5	51.7	5.43
13*	CU	14	5	8.25	Bearing	9	8	8.5	68	40	8.5	52.0	4.95
14	USC	15	5.5	8.25	Bearing	9.5	8.5	8.5	72.25	40	8.5	51.7	5.43
15*	USC	14	5	8.25	Bearing	9	8	8.5	68	40	8.5	52.0	4.95
16	USC	15	5.5	8.25	Bearing	9.5	8.5	8.5	72.25	40	8.5	51.7	5.43
17	USC	15	5.5	8.25	Bearing	9.5	8.5	8.5	72.25	40	8.5	51.7	5.43
18*	CU	14	5	8.25	Bearing	9	8	8.5	68	40	8.5	52.0	4.95
19*	CU	14	5	8.25	Bearing	9	8	8.5	68	40	8.5	52.0	4.95
20*	USC	14	5	8.25	Bearing	9.5	8.5	8.5	72.25	40	8.5	51.7	4.95

**Test No. 7 is the flat slab with two C channels on the top.*

**Test No. 8 is the flat slab with two steel plates on the top.*

**Test No. 9 is the flat slab with plates from bottom.*

**Test No. 13 is the flat slab with plates from bottom.*

**Test No. 15 is the flat slab with external post tensioning.*

**Test No. 18 is the flat slab with plates from bottom.*

**Test No. 19 is the flat slab with plates from bottom.*

**Test No. 20 is the near surface mounted bars.*

L	Length of Slab	ft		a	Length of bearing pad	in
D	Depth of Slab	in		b	Width of bearing pad	in
E	Width of Slab	ft		c	Distance of center to center from one bearing pad to the other	in
W	width of the bearing	in		d	Width of spreader beam	in
A	Surface area of bearing pads on the spreader beam (neoprene pad)	in^2		X	Shear span length (distance of loading point from the supports)	ft
F	Length of spreader beam	in				

Figure 3.3 Flat slab test setup; left) University of South Carolina, right) Clemson University.

3.1.2 Strengthened slab from above

Two methods of strengthening from above were investigated for a single slab span. Two A36 steel C10x15.3 channels anchored to the slab surface were tested to failure. Two A572 steel plates were also anchored to the slab surface and were tested to failure. Strengthening from the slab surface was considered for its ease of access and constructability reasons. Strengthening from the surface has the potential to save costs of construction if the bridge location has natural obstacles preventing access to the bottom of the slabs. One drawback of this approach is the requirement of an asphalt overlay layer to cover the anchored steel for a suitable driving surface. Steel anchored to the surface may also trap moisture underneath the asphalt layer and cause corrosion. Photographs of the strengthened slab with two C-channels and two steel plates are shown in Figures 3.4 and Figure 3.5. Strengthening from above with near surface mounted (NSM) bars was also investigated and is summarized in Section 3.1.5.

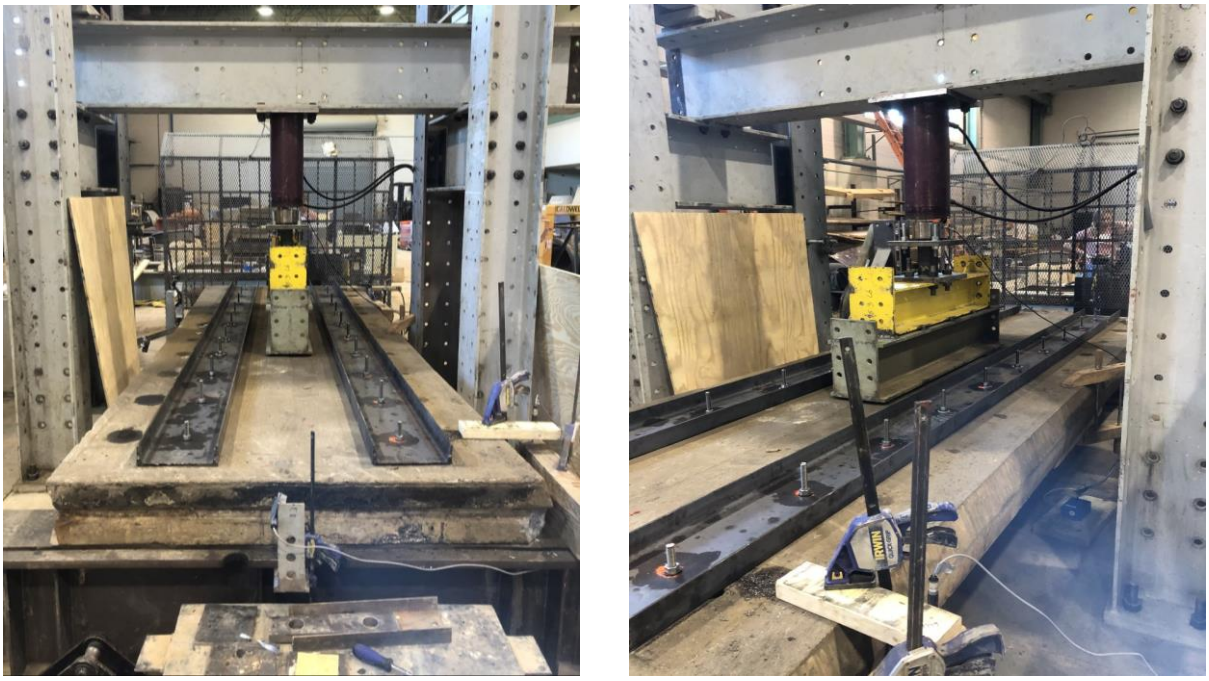

Figure 3.4 Strengthened slab test setup with two steel channels on top.

Figure 3.5 Strengthened slab test setup with two plates on top.

Details of the channels are shown in Figure 3.6. The channels had a specified yield strength of $f_y = 36000psi$. Adhesive anchors with a drilled hole diameter of 3/4 in. were used to anchor the 5/8 in. diameter threaded rod at an embedded depth of four inches into the concrete. DeWalt Pure 110 + was the adhesive selected for anchoring. Instructions for installation of the Pure 110+ anchoring adhesive were followed, and a representative of DeWalt provided in-person training for the individuals installing the anchors. Holes through the steel channels were 7/8-inch in diameter to allow tolerance for the anchor and hole locations.

Details of the steel plates are shown in Figure 3.7. The steel plates specified yield strength of $f_y = 70000psi$. The steel plates are the same length as the steel channel. Adhesive anchors with a drilled hole diameter of 3/4-inch were used to embed the 5/8-inch diameter threaded rods at a depth of four inches with DeWalt Pure 110+ adhesive as the anchor. Instructions for installation of the Pure 110+ anchoring adhesive were followed identically to the steel channel assembly described above. Holes through the steel plates were 3/4-inch diameter to minimize changes in annular distance between the threaded rod and steel hole.

A combination of string potentiometers and LVDT sensors were used to measure vertical displacement at mid-span and horizontal displacement at the slab ends. The load was applied using a hydraulic actuator, and a calibrated load cell and pressure gage was used to track load during the test. Specialized and dedicated data acquisition systems were used to record data continuously. The test configurations and connection details are shown in Figure 3.8, Figure 3.9, and Figure 3.10.

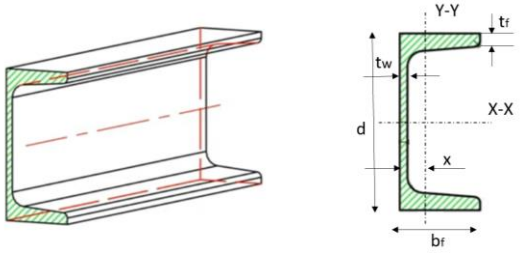

American Standard Steel C Channel Sizes													
Designation	Area, A, (in^2)	Depth, d, in	Weight, lb/ft	Flange		Web Thickness t_w, in	Axis X-X			Axis Y-Y			X, in
				Width, b_f, in	Thickness, t_f, in		I, in^4	S, in^3	r, in	I, in^4	S, in^3	r, in	
C10X15	4.49	10.00	15.3	2.6	0.436	0.24	67.4	13.5	3.87	2.28	1.16	0.713	0.634

Figure 3.6 Channel size chart for dimensions, weight, and section properties of steel channels.

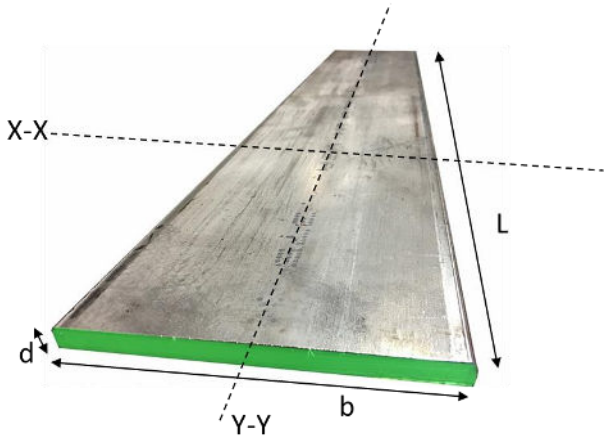

Designation	Area, (in^2)	Length, In	Width, b, in	Weight, lb/ft	Thickness, d, in	Axis X-X	Axis Y-Y	Yield strength (ksi)
						I, in^4	I, in^4	
ASTM A572 Grade 55	8	160	16	34	0.5	0.167	170.67	70

Figure 3.7 Steel plate size chart for dimensions, weight, and section properties.

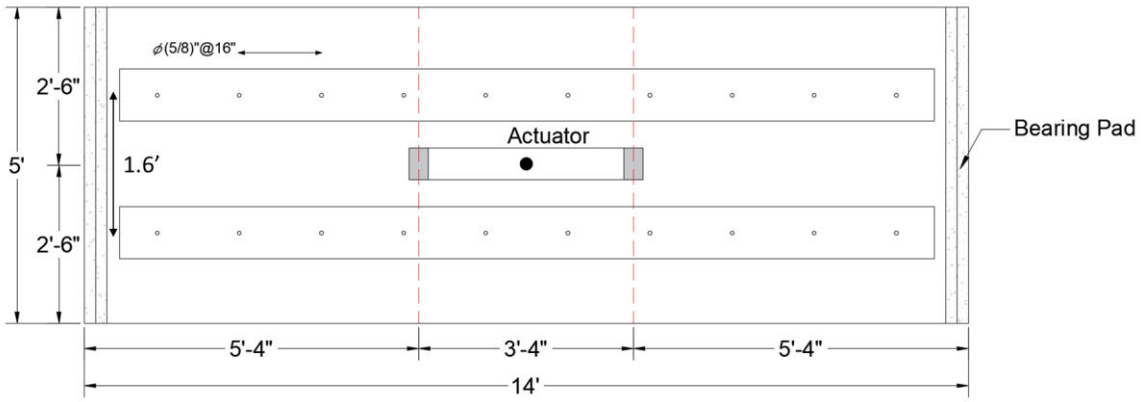

Figure 3.8 Plan view of the strengthened C-channel slab test setup.

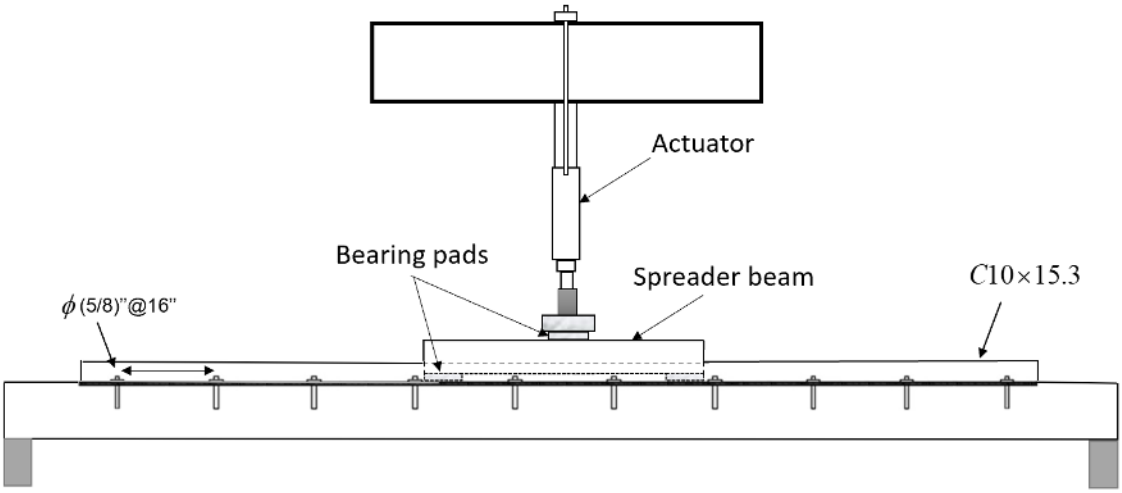

Figure 3.9 Side view of the strengthened C-channel slab test setup.

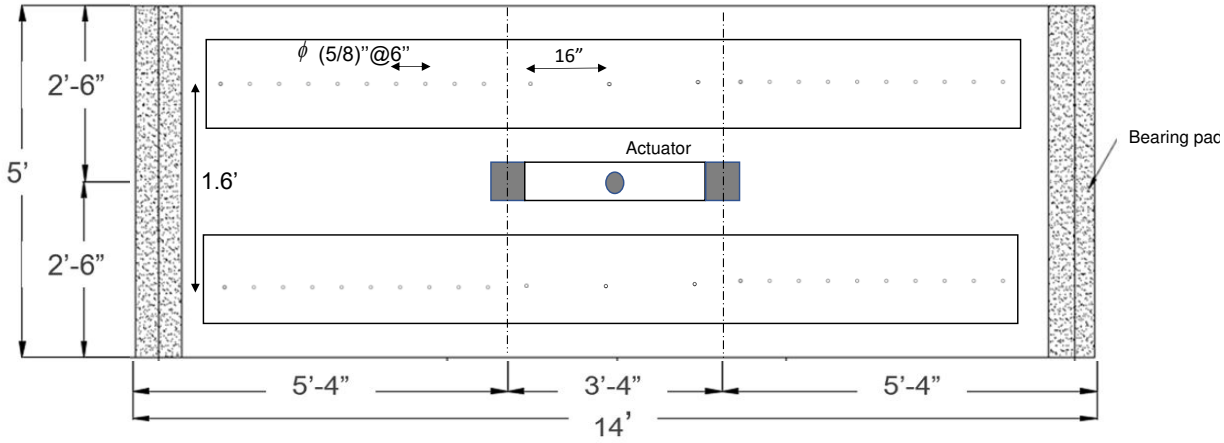

Figure 3.10 Plan view of the strengthened slab with steel plates test setup.

3.1.3 Strengthened slab from bottom

This strengthening method involved bolting steel plates to the slab bottom, with the steel plates acting as external tension reinforcement for the slab. The four plate configurations and respective number of bolts, along with sizes and grades used, are shown in Table 3.4. All plates had a specified yield strength of $f_y = 36000psi$. Results of steel coupons tested after the initial test are shown in Table 3.5.

Prior to the first three strengthening methods, Ground Penetrating Radar (GPR) was used to locate flexural steel and to determine the size of the rebar. These locations were then marked and used to coordinate hole drilling locations to avoid damaging any flexural steel. While GPR was not used on the 4th method, no flexural rebar was cut in the drilling process. The slab was core drilled with a two-inch bit 8 in. on center longitudinally on the slab. The center of the first hole began 1 ft. 10 in. from the edge of the slab. The plates were prepared with rope caulk around the holes to create a seal between the steel and the concrete slab and were held in place with 2 x 6 transverse wood planks at 1/3 points longitudinally (Figure 3.11). Bar clamps were used to hold the wood, and,

consequently, the plates in place. With the plates secured, the bolts were then positioned in each of the holes. The holes were filled with non-shrink grout, which set for 24 hours before the wood and bar clamps were removed. The grout cured for 7 days in the slab before the first test. For the next three tests, the grout was cured in the slab for 48 hours before testing. The experimental tests of the grout strength are shown in Table 3.6. Grout cubes were made from each batch and tested to determine the compressive of the grout used. All tests were performed according to ASTM C 109 and the results shown are an average of 2 or 3 tested grout cubes.

The test setup consisted of a reaction frame, a hydraulic actuator, and a spreader beam used to distribute the load. Figure 3.12 shows the test setup of the first strengthening attempt. The second, third, and fourth methods used the same setup, just having fewer holes than is shown. Three wire potentiometers were set up under the slab at midspan, one was placed in the middle of the slab and the others were on either outer edge of the slab. The wire potentiometers at midspan were used to measure the vertical deflection. Another wire potentiometer was placed where the slab rested on the bearing pad to measure the compression displacement of the bearing pad on the first method. Two strain gauges were placed on each steel plate at midspan to measure the strain in the external steel. The load was measured using a pressure gauge that was in line with the supply for the hydraulic actuator. The measured pressure was multiplied by the actuator area to determine the applied load. Data from all instruments were continuously monitored and recorded during testing. Figure 3.13 shows the instrumentation set up in the lab from both the side and from below for the first method. Like the previous figure, the setup remained the same in subsequent methods, but the bolts and plates were adjusted according to Table 3.4.

Table 3.4 Details of strengthening schemes. Variables included the quantity and size of plates and the quantity and size of bolts.

	Side View

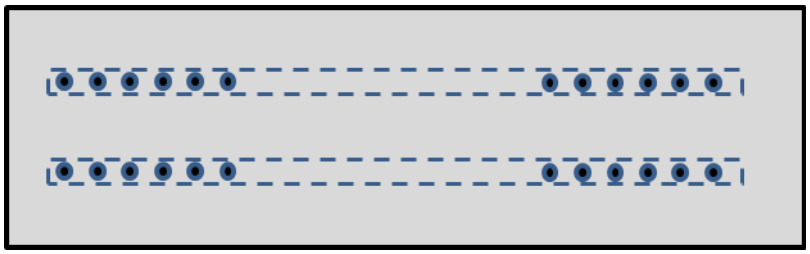	Method 1 (2) 3” x 1/2” Plates attached at 1/4 points from edge (6) 5/8” Ø A307 Bolts on either side of each plate Bolt Shear Failure
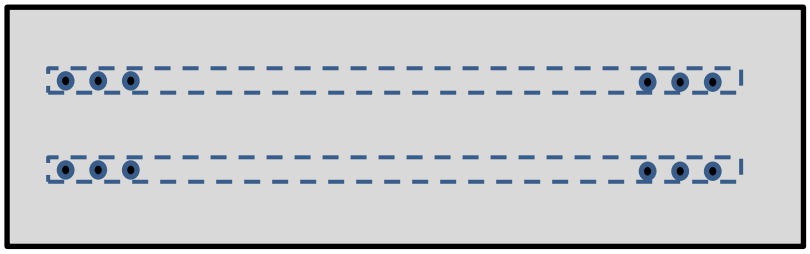	Method 2 (2) 3” x 1/2” Plates attached at 1/4 points from edge (3) 3/4” Ø Grade 8 Bolts on either side of each plate Flexural Failure
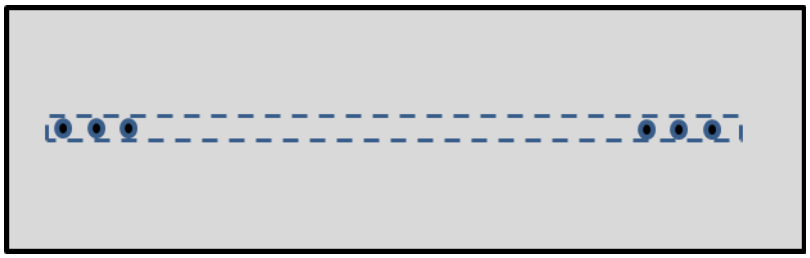	Method 3 (1) 3 3/4” x 1/2” plate attached at midpoint (3) 3/4” Ø grade 8 Bolts on either side of each plate Flexural Failure
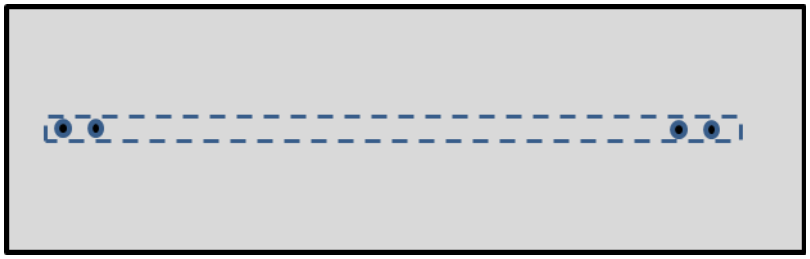	Method 4 (1) 2 1/2” x 1/2” plate attached at midpoint (2) 3/4” Ø Grade 8 bolts on either side of each plate Flexural Failure

Table 3.5 Tensile strength of 4 steel plate specimens per ASTM E 8

	Yield Stress (ksi)	Ultimate Stress (ksi)
Average Tested	51.0	69.0
Minimum Tested	48.2	68.3
Maximum Tested	51.0	70.5
Specified	36.0	58.0

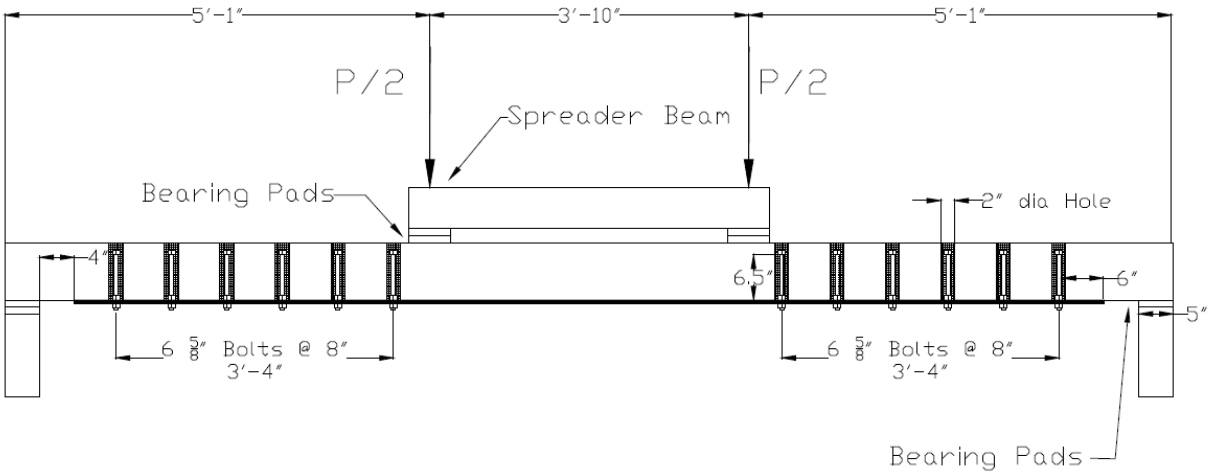

Figure 3.11 Side view of the strengthened slab for method 1. Other methods used the same load and support geometry.

Table 3.6 Average compressive strength of grout cubes

	Data Sheet (psi)	Method 1 (psi)	Method 2 (psi)	Method 3 (psi)	Method 4 (psi)
1 Day	3500	2600	3000	3100	2100
2 Days	—	—	4700	5000	4000
7 Days	5700	6900	5700	6400	6800
28 Days	6200	7200	8400	8000	8500

Figure 3.12 Installation of bolts and grout of the strengthened slab with steel plates from bottom. Wood planks, clamps, and grout are shown in the left photo; hole cutting is shown in the right photo.

Figure 3.13 Strengthened slab test setup and ready for loading (left). Two plates installed on bottom of slab (right).

3.1.4 External Post Tensioning from below

The slab was strengthened by external post tensioning of DYWIDAG threadbars at the bottom of the slab. A rotary hammer drill and 1-inch drill bit were used to drill 6 through-holes 6 in. on center along the transverse direction on both sides of the slab. The first hole began 1 ft. from the width and 1 ft. 6 in. from the edge of the slab (Figure 3.14). 1/2 in. thick steel plates with 3 ft. length and 6 in. width were aligned along the holes and held in place using 7/8 in. diameter and 1ft. length high strength threaded rods on either side of the slab. The first hole in the steel plates started 3 in. from the edge of the plate in the longitudinal direction. Steel plates used on top of the slabs and threaded rods had a specified yield strength of $f_y = 36000$ psi and $f_y = 75000$ psi, respectively. Clamps and a hydraulic jack were used to hoist the steel angles up toward the bottom of the slab and properly align to the threaded rods. L 6 x 6 x 1 steel angles had a specified yield strength of $f_y = 36000$ psi and were strengthened by welding square steel shapes to the inside of the legs to prevent any yielding. The first hole in the steel angle began at 3 in. from the edge of the horizontal leg in the longitudinal direction. The configuration of steel plates and steel angles placed on the slab are shown in Figure 3.15. Three 5/8 in. diameter DYWIDAG threadbars were suspended at 1 ft. spacing through the vertical legs of the steel angles at the bottom of the slab. First hole was drilled at 6 in. from the edge on the vertical leg along longitudinal direction of the steel angle. The threadbars had a specified ultimate strength of 160,000 psi. The properties of DYWIDAG threadbars are presented in Table 3.7 (DYWIDAG threadbars – Technical Data,2014). Hex nuts were used to keep the prestressing bars in place and apply post tension force in the bars. Strain gauges were attached to the bars to measure the strain in the bars and calculate the prestressing force produced in the bars. Hex nut on one side was kept fixed by placing a wrench. Wrenches were used to manually twist the nuts on both ends applying torque to produce tension force in the bars. An average strain of 1100 με was obtained producing a prestressing of 32,000 psi in the bars. No loss in prestressing was observed when the strains were checked before testing the slabs.

Table 3.7 Specified Properties of DYWIDAG threadbars

Steel Grade 160 ksi	Nominal Bar Diameter, in	Steel Area in^2	Yield Load $Py=f_yA_s$ kips	Ultimate Load $Pu=f_uA_s$ kips	Nominal weight lbs/ft	Mill length ft	Direction of Thread L or R
Hot-Rolled Threaded bar (post-tensioning)	5/8	0.27	35.7	43.6	0.99	19.3	R

The process of post tensioning and the test setup prior to loading are shown in Figure 3.16. The simply supported slabs rested on neoprene pads above the steel beam. Strain gauges were attached to the external thread bars to assess the prestressing force. A combination of string potentiometers and LVDTs were used to measure the vertical deflection at mid-span of the slab and a hydraulic actuator was used to apply incremental load. A load cell and a pressure gauge were used to monitor load during the test. BDI strain gauges were used to record bending strain on the wearing surface of the slab at midspan during loading. Specialized and dedicated data acquisition systems were used to continuously record the readings of strain gauges, LVDTs, and the load cell. Details of the strengthening scheme are shown in Table 3.8.

Table 3.8 Details of strengthening scheme

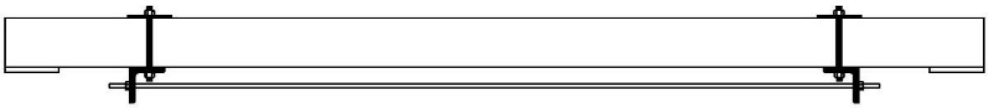	Side View
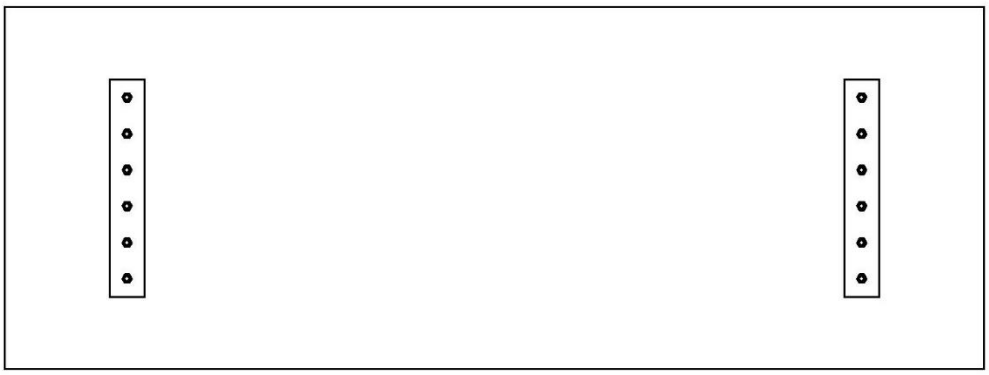	(2) 6” x 36”- 1/2” thick plates attached on top of the slab (12) 7/8” Ø F1554 Grade 55 Bolts inserted through the slab
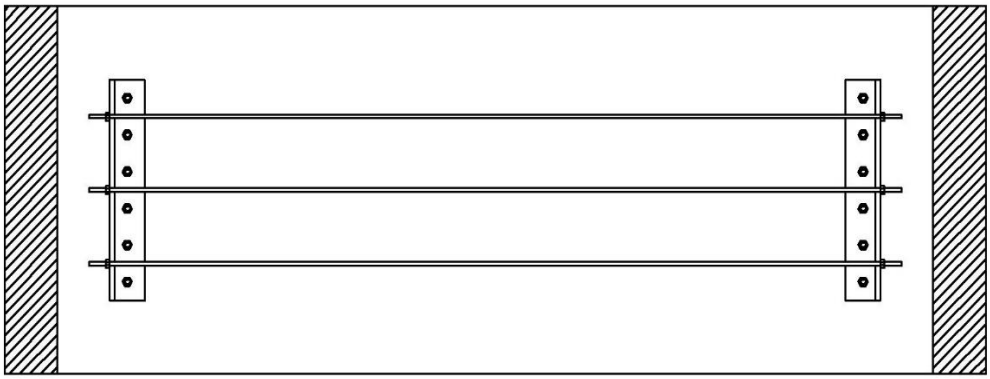	(2) L6x6x1 steel angles 3 ft length held on both sides (3) 5/8” Ø DYWIDAG threadbars GR 160, 12 ft. long suspended through steel angles

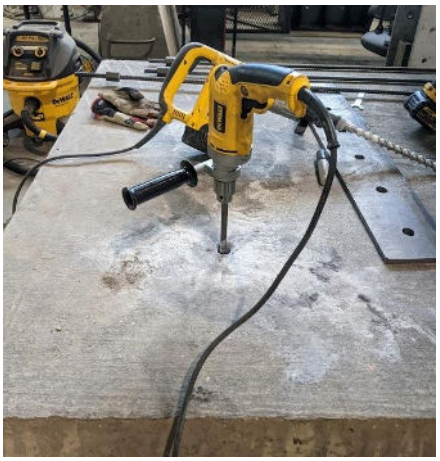
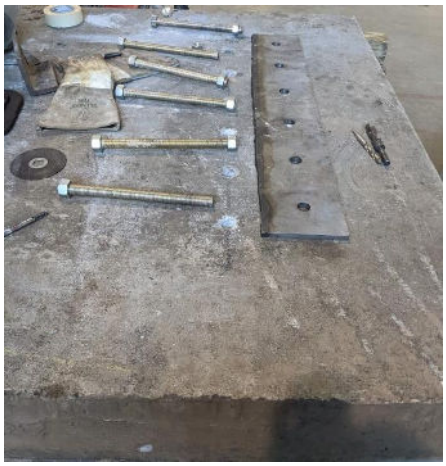

Figure 3.14 Hammer Drilling (left) and threaded rods and steel plate ready to be placed on the slab (right).


Figure 3.15 Installation of steel plates (left) and installation of steel angles and DYWIDAG threadbars (right).

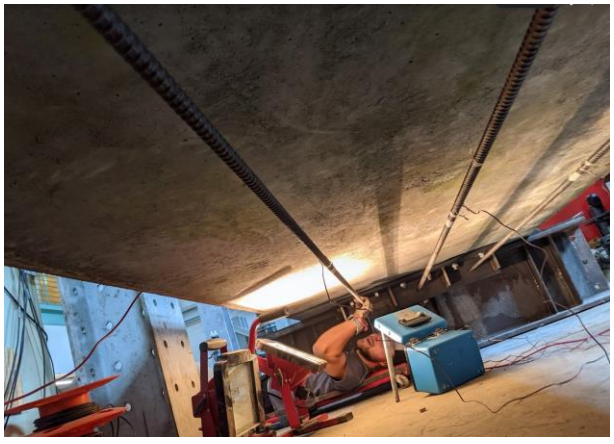


Figure 3.16 Post tensioning DYWIDAG threadbars (left), Strengthened slab test setup ready for loading (right).

3.1.5 Near-surface-mounted

A near-surface-mounted technique was investigated to transform the two simply supported slab spans into one continuous span and was tested to failure. Two 14 ft. by 5 ft. slabs in series were clamped with a transverse tie rod at the joint and supported at the joint and at opposite ends of both slabs. Two steel plates and two hex nuts were used to clamp the sides of the slabs together. The hex nuts were tightened as much as possible using a 2 ft. wrench. The goal of this testing setup was to mimic the actual conditions of observed flat slab bridge joints in South Carolina. Six 2 in. by 2 in. by 10 ft. grooves were cut with a concrete wet saw, then chipped out using a rotary hammer drill as shown in Figure 3.17. Dust and debris were removed, and 6 #6 steel bars 10 ft. in length were placed into the grooves and covered with Sakrete non-shrink construction grout. The reinforcement bar grade is 60,000 psi, and the 28-day compressive strength for Sakrete grout is 8000 psi. Grooves were in a saturated surface dry condition when the grout was applied as per Sakrete installation instructions. Strain gauges were placed at two different locations on the steel bars: directly over the joint and 20 in. from the edge on the loaded slab (Figure 3.18). The Testing set up is depicted in Figure 3.19. The orientation of the transverse tie rod is shown in Figure 3.20.

A combination of string potentiometers and LVDTs was used to measure the vertical deflection at mid-span of the slab and a hydraulic actuator was used to apply incremental load. A steel spreader beam was utilized to distribute the load on the slab. A load cell and a pressure gauge were used to monitor load during the test. Specialized and dedicated data acquisition systems were used to continuously record the readings of strain gauges, LVDTs, and the load cell.

Figure 3.17 Concrete grooves cut into slab and over joint

Figure 3.18 Placement of #6 Bars and Strain Gauges

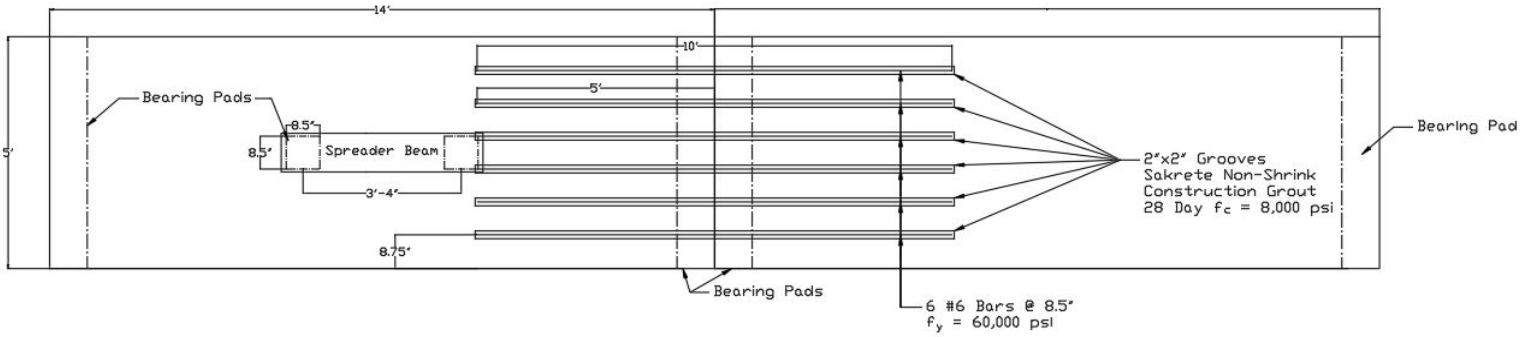

Figure 3.19 Plan view of test setup

Figure 3.20 Transverse tie rod for clamped connection of slabs in series

3.2 Numerical modeling of flat slabs

A numerical model of the flat slab test was generated in the commercial FE program ABAQUS to evaluate the moment capacity of the flat slab with steel channel strengthening, with steel plate strengthening, and without any strengthening. The slab and channel were modeled with 8-node linear brick elements having reduced integration (C3D8R) and the rebar was modeled with 2-node linear elements (B31). The typical mesh size of the concrete was three cubic inches. Details of the model are provided in Figure 3.21. The area of the contact surface is 144.5 in.^{2}. To be consistent with the laboratory tests, the same pressure and load were applied in the FE model on the contact surface in the positions shown in Figure 3.21.

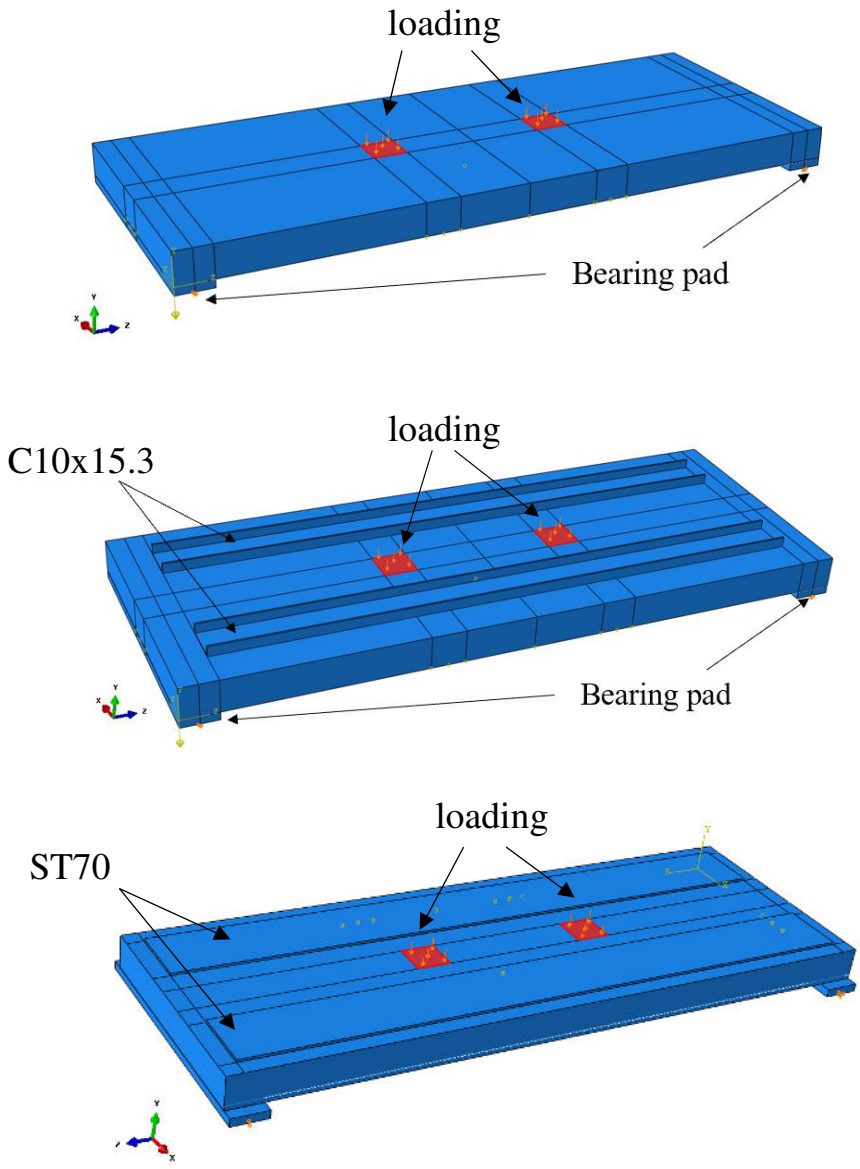

Figure 3.21 FE modeling of precast reinforced flat slabs with and without strengthening.

The Young's modulus was taken as 29,000,000 psi, with yielding stress of 36,000 psi for the steel channels, yielding stress of 70,000 psi for the steel plates, and 60,000 psi for the steel reinforcement. The Young's modulus of concrete in the model was assumed to be 3,605,000 psi. The constitutive law of concrete employed in the model representing compressive and tensile damage is shown in Figure 3.22.

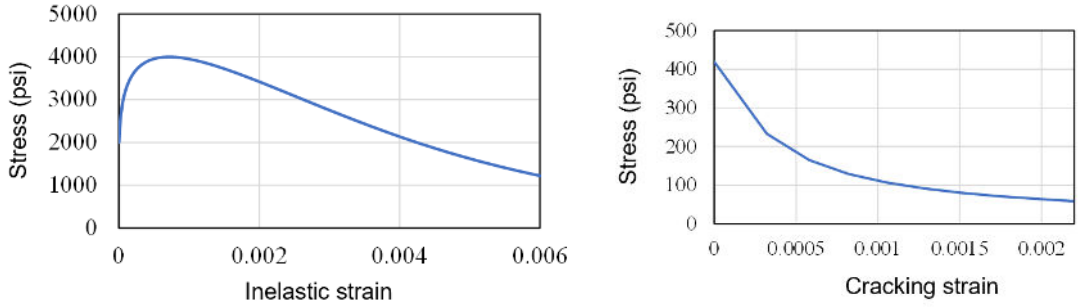

(a) (b)

Figure 3.22 Constitutive law of concrete damage: (a) compressive; (b) tensile.

3.3 Development of CNN models for inspection

Autonomous inspection implementing a deep learning model was developed to detect the presence of the cracks and determine their severity of the damage without the need of physical human inspection. A deep learning model consists of an input layer, a CNN architecture, and an output layer. The images of concrete surface with their respective labels are fed into the model as an input, the CNN model extracts the features from the image using convolution and pooling layer. Classification of the image is done in fully connected layer and an output layer. The output layers classify the images and assign the labels to the input images. The performance of the model is evaluated in terms of a confusion matrix.

Two CNN models are developed to detect the presence of the cracks and determine the severity of the damage. Image database is required to train and test the model to obtain an accurate and optimized model. For the CNN model for crack detection, image database is obtained from a public dataset. However, image database for damage severity could not be found, so an image database was first generated. Images from a slab were taken using a drone. The depths of the cracks were measured. These images taken from the slab were preprocessed to obtain a larger database. This image database is used for training and testing the CNN models.

3.3.1 Image database for crack detection and to determine damage severity

A CNN model is developed by training the model to a large input database of images collected from ImageNet database. The database consists of 40,000 images of concrete surfaces. These images are divided into two sets, images without cracks named as "Undamaged," and the images with cracks named "Crack" as shown in Figure 3.23. These images will be fed to the CNN model as an input for training and testing the model.

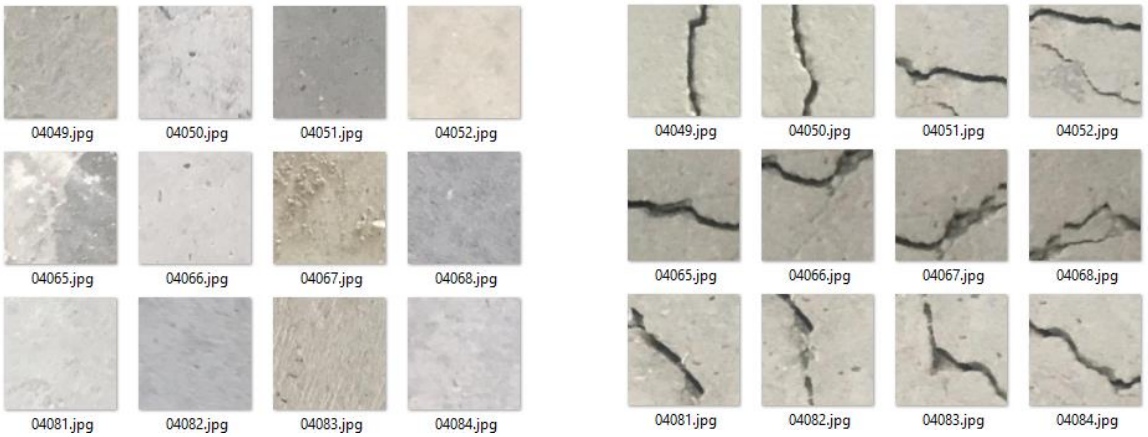

(a) (b)

Figure 3.23 Images of the concrete surface (a) Undamaged (b) Crack

A multi-class CNN model is developed to determine the damage severity of the cracks based on the crack depth. An image database was generated from a slab specimen at USC for the multi-class CNN model. The slab has multiple cracks with varying lengths and depths on its surface as shown in Figure 3.24. Images of the cracks were taken using a Parrot ANAFI drone (Figure 3.25) at one foot from the surface of the slab. Data augmentation is applied to generate the substantial number of images in the database.

Figure 3.24 Damage slab specimen

Figure 3.25 Parrot ANAFI drone

The maximum depth of the crack along the length of the crack was measured using a scale and paper to generate an image database as shown in the Figure 3.26. The images of the cracks were classified to three zones based on their depths. The images of the cracks with depth less than 1 cm were labelled as Zone 1, images of the cracks with a depth of more than 1 cm and less than 2 cm were labelled as Zone 2 and the images of the crack with a depth of more than 2 cm were labelled as Zone 3 (Table 3.9).

Figure 3.26 Imaged database for damage severity

Table 3.9 Damage zones based on the damage severity

Damage zone	Depth range (cm)
Zone 1	≤ 1.0 cm
Zone 2	> 1 cm and ≤ 2.0 cm
Zone 3	> 2.0 cm

3.3.2 Development of the CNN models

A CNN model is developed for the binary classification of cracks through feature extraction to identify the presence of a crack in an image (Figure 3.27). It is trained through images containing cracks and images without cracks. The model will be able to classify the images to "undamaged" and "crack" labels. After training the model, people with little knowledge of machine learning are still able to utilize the model which makes this method easy to be used in the field.

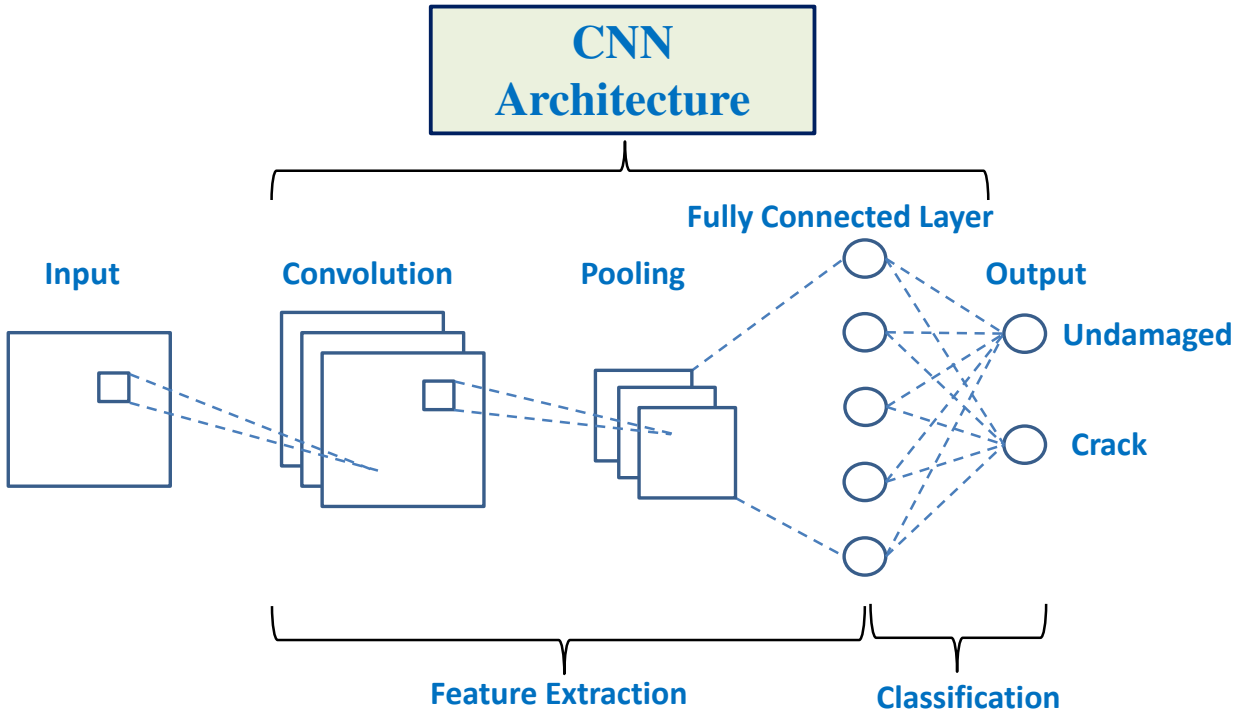

Figure 3.27 A CNN model for crack detection

After identification of the cracks, multi-class CNN model is developed for the classification of various levels of damage zones to be assigned to each crack (Figure 3.28). Damage levels are assigned based on the depth of the crack. This provides an insight on the severity of the cracks, the higher the depth of the crack higher the damage severity. The multi-class CNN model is trained to recognize the severity of the crack and classify the images to their respective damage zones, Zone 1, Zone 2, and Zone 3.

The images with their respective labels based on the depth of the crack were input to the multiclass CNN model. The CNN model extracts the features and classifies the images to their respective zones. The performance of the multiclass model is evaluated using a confusion matrix.

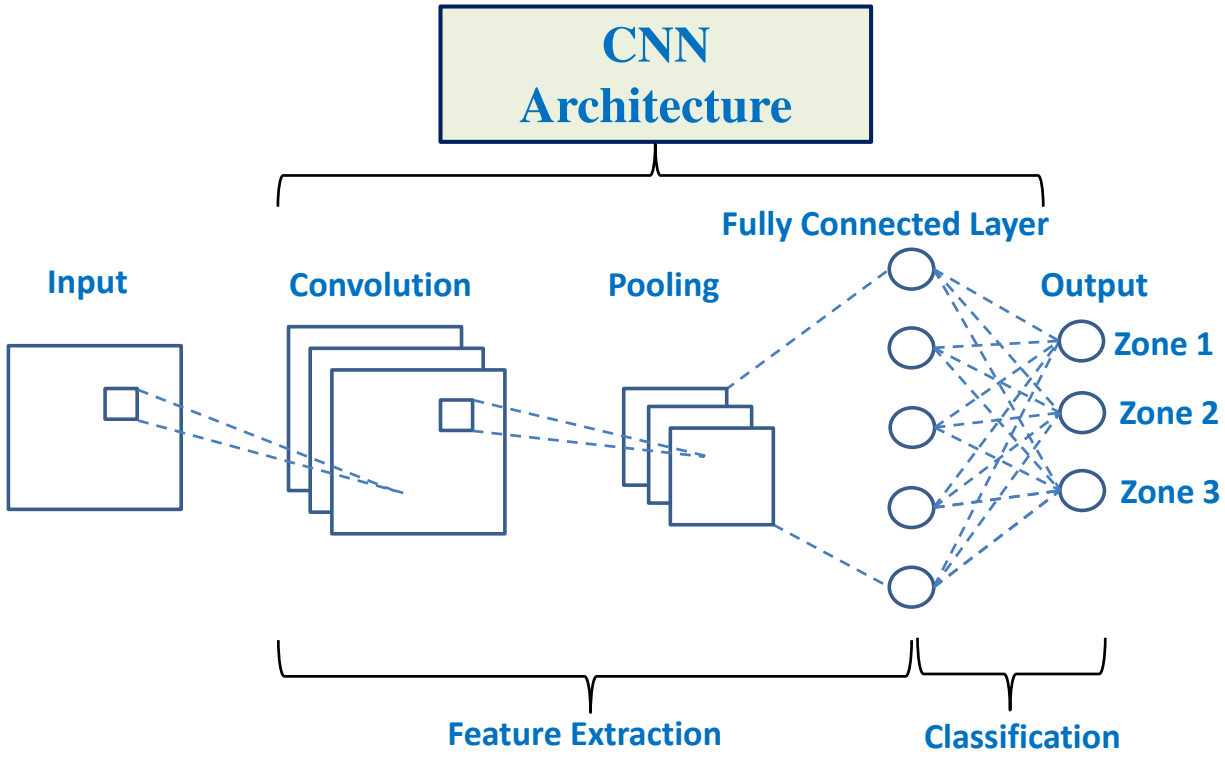

Figure 3.28 A multiclass CNN model for classification of the crack

CHAPTER 4: RESULTS

A discussion of test results for the baseline (unstrengthened) and strengthened precast, reinforced concrete flat slabs is presented in this chapter.

4.1 Baseline Flat Slab Results

Moment versus vertical displacement of the baseline (unstrengthened) 14 ft. and 15 ft. long flat slab specimens are shown in Figure 4.1 and Figure 4.2, respectively. The moment in the figure includes the dead weight effects of the slab and the moment from the applied load. The general shape of the moment versus deflection plots of the unstrengthened slabs can be divided into three linear segments and is as expected: zero load to first cracking, first cracking to first yield of reinforcement, and first yield to flexural failure. Flexural failure of the specimens was characterized by yielding of the reinforcement and crushing of the concrete in the maximum moment region (Figure 4.3). Tables 4.1 and 4.2 summarize the test results for the 14' and 15' long slabs, respectively. The average measured Moment Capacities for the baseline slabs are 208 kip-ft for the 14' long slabs and 228 kip-ft for the 15' long slabs. It should be noted that average 15' long slabs failure moment does not include the result from test 4 due to inconsistencies from the roller bearing support condition. The calculated Yield Moment & Moment Capacities in Tables 4.1 and 4.2 were determined using conventional reinforced concrete strength design concepts with specified concrete and steel material properties.

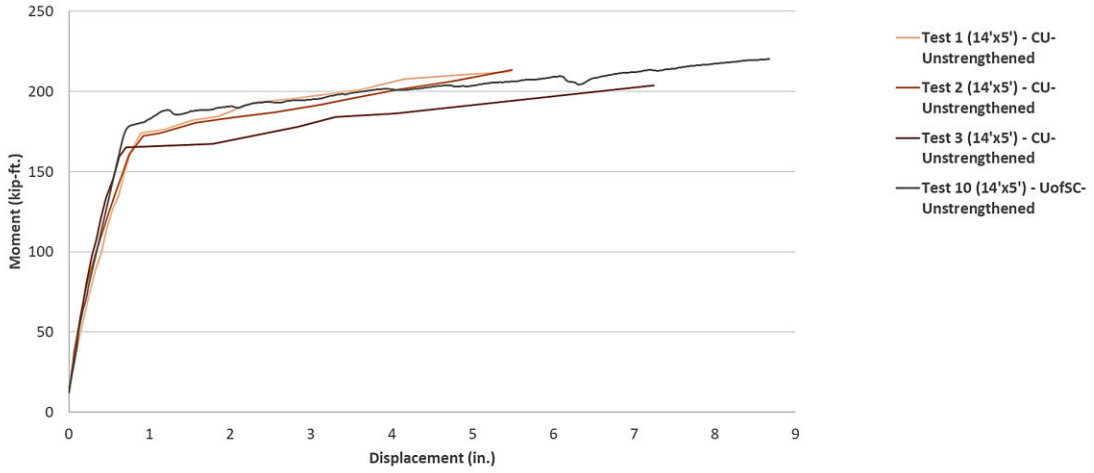

Figure 4.1 Total moment vs. vertical displacement for 14' long slabs.

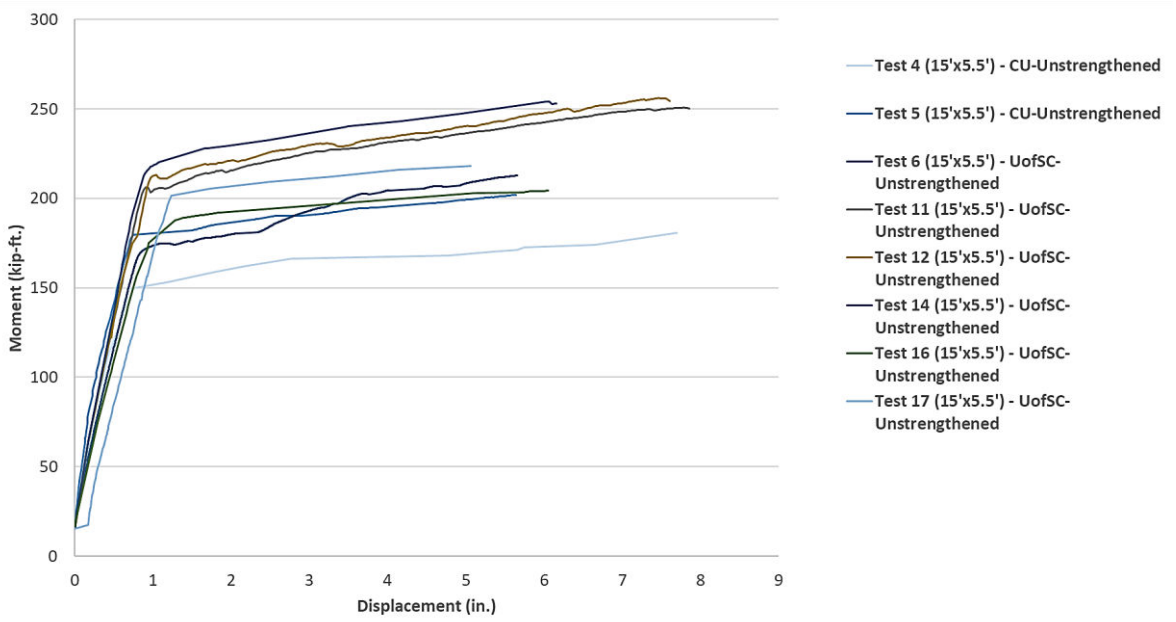

Figure 4.2 Total moment vs. vertical displacement for 15' long slabs.

Figure 4.3 Deformation (left) and concrete crushing (right) of the flat slabs.

Table 4.1 Unstrengthened Slab Flexural Test Results – 14' long

Test #	Calculated Yield Moment (kip-ft)	Calculated Moment Capacity (kip-ft)	Measured Yield Moment (kip-ft)	Measured Moment Capacity (kip-ft)	Measured Yield Moment/Calculated Yield Moment	Measured Moment Capacity/ Calculated Moment Capacity	Failure Mode
1	107	123	174	212	1.63	1.72	*
2	107	123	172	213	1.61	1.73	*
3	107	123	167	204	1.56	1.66	*
10	107	123	161	201	1.50	1.63	*
*Crushing of concrete due at slab surface due to flexural compression Note: Calculated Moments are derived from SCDOT specified material properties							

Table 4.2 Unstrengthened Slab Flexural Test Results – 15' long

Test #	Calculated Yield Moment (kip-ft)	Calculated Moment Capacity (kip-ft)	Measured Yield Moment (kip-ft)	Measured Moment Capacity (kip-ft)	Measured Yield Moment/Calculated Yield Moment	Measured Moment Capacity/ Calculated Moment Capacity	Failure Mode
4**	117	136	149	180	1.27	1.32	*
5	117	136	179	202	1.53	1.49	*
6	117	136	171	215	1.46	1.58	*
11	117	136	204	250	1.74	1.84	*
12	117	136	213	256	1.82	1.88	*
14	117	136	219	253	1.87	1.86	*
16	117	136	187	204	1.60	1.50	*
17	117	136	204	218	1.74	1.60	*
*Crushing of concrete due at slab surface due to flexural compression ** Denotes a pin and roller boundary condition instead of normal bearing conditions Note: Calculated Moments are derived from SCDOT specified material properties							

4.2 Strengthened Flat Slab Results

Four strengthening strategies were used: a) Attachment of steel sections to the top of the bridge deck: strengthening was accomplished by either attaching two C10 x 15.3 channels to the top, or by attaching two 0.5 in. x 16 in. plates attached to the top of the slab, b) attachment of steel plates to the bottom of the bridge deck: strengthening from below was achieved by attaching plates on the bottom of the slab using four variations of plate size and attachment schemes, c) external post-tensioning attached to the deck bottom: strengthening by external post tensioning was achieved by suspending and prestressing three 5/8 in. diameter DYWIDAG threadbars between two steel angle sections attached to the bottom of the slab, and d) near-surface mounted bars (NSM): #6 bars were embedded into the surface of two slabs in series to create one continuous slab with two unsupported spans. It should be noted that all strengthened slabs were 14 ft. long, and, therefore, were only compared to the results from 14 ft. long unstrengthened slabs.

Figure 4.4 shows a comparison of the flexural behavior of all 14 ft. slab tests (unstrengthened and strengthened). The behavior of all slabs was effectively linear until the moment reached a minimum of 170 kip-ft. After the yielding of the internal reinforcement the stiffness of the specimens reduced. The slab strengthened using post-tensioning from below had the highest moment capacity, but less ductility than the slabs strengthened from above.

The average measured moment capacity of the baseline 14 ft. long flat slabs is 208 kip-ft. and was used for comparison with strengthened slabs that are shown Table 4.1. Strengthening from above with the two channels improved peak experimental capacity by 12% relative to the baseline specimen. Strengthening with two channels also significantly increased ductility, achieving a 230% increase in midspan deflection at failure compared to the baseline. Strengthening from above with the two steel plates improved peak measured capacity by 4% relative to the baseline specimen. Two plates on top also increased ductility by 73% compared to the baseline average midspan deflection. The strengthening from below with steel plates increased the moment capacity by 13% or more. The slab strengthened from the bottom in method 1 does not follow the trend of the others because the bolts underneath the slab holding the steel in place sheared. The test was stopped after shearing of the anchoring bolts and shows a quasi-brittle behavior at a peak moment of 240 kip-ft. Methods 2 through 4 achieved flexural failures after reaching yield moments of 200 kip-ft, 182 kip-ft, and 164 kip-ft. After the slabs reached these moments, they were able to support greater deflection comparatively, but minimal additional moments until they reached peak capacity, where the compression zone crushed. Peak capacity for each slab was 252, 293, 268, and 236 kip-ft, respectively, for methods 1 through 4. As with the baseline slabs, all slabs experienced crushing in the maximum moment region, near the midspan. While the strengthened slabs experienced higher flexural strengths, the ductility slightly decreased. Despite this ductility decrease, all slabs still maintained tension-controlled behavior.

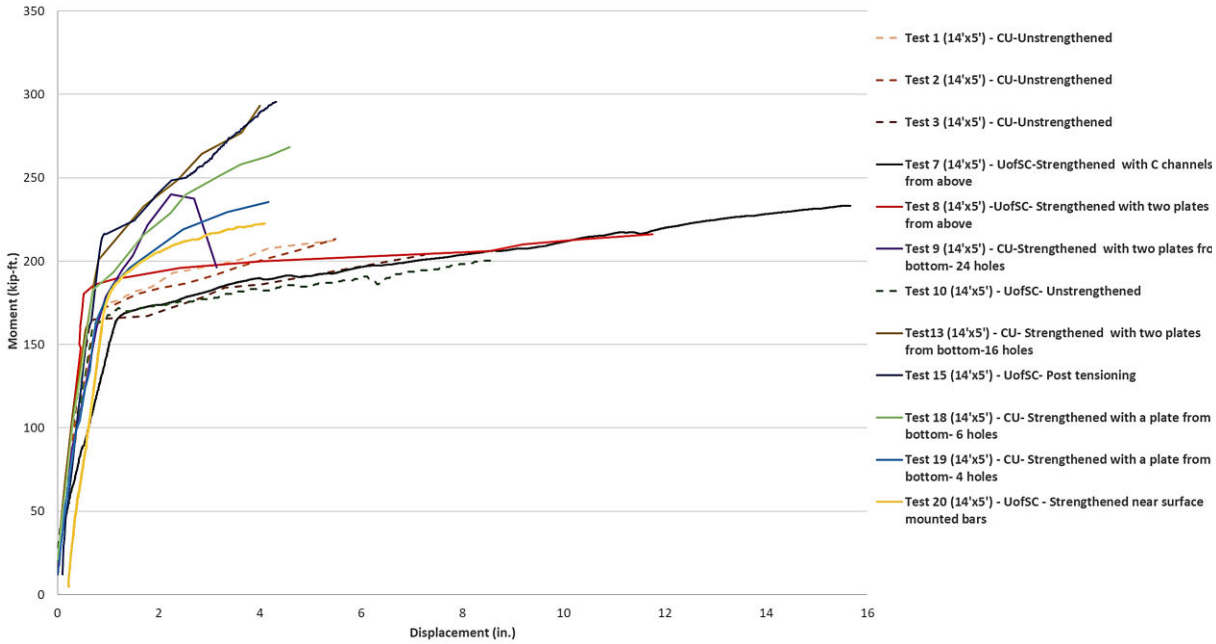

Figure 4.4 Total moment vs. vertical displacement for strengthened and unstrengthened 14' slabs.

Table 4.3 Comparison of baseline and strengthened 14' long slabs

	Measured Yield Moment (kip-ft)	Measured Moment Capacity (kip-ft)	Measured Yield Moment/ Baseline Yield Moment	Measured Moment Capacity/ Baseline Moment Capacity	Failure Mode
Average of Baseline specimen (Unstrengthened)	169	208	N/A	N/A	Flexure
Strengthened with channels from above	167	233	0.99	1.12	Flexure
Strengthened with steel plates from above	185	217	1.09	1.04	Flexure
Strengthened with steel plates from below: Method 1	190	252	1.12	1.21	Bolt Shear
Strengthened with steel plates from below: Method 2	200	293	1.18	1.41	Flexure
Strengthened with steel plates from below: Method 3	182	268	1.08	1.29	Flexure
Strengthened with steel plates from below: Method 4	164	235	0.97	1.13	Flexure
Strengthened with external post tensioning	216	296	1.28	1.42	Flexure
*N/A refers to not applicable.					

4.3 FE Analysis of Test Results

The experimental strength of the baseline slab was compared to the calculated (nominal) capacity. Nominal capacities were calculated using classical flexural theory and assuming *f'c = 4,000 psi* and *fy = 40,000 psi* or *60,000 psi*. The nominal capacity for the first scenario was 64% of the experimental moment, whereas the nominal capacity obtained using the second scenario was 91% of the experimental moment. This supports the theory that the reinforcement in the slab is in the range of 60,000 psi, however other factors including partial arching action due to horizontal restraint at the supports and concrete compressive strength more than 4,000 psi may also play a role.

To further evaluate the behavior of the flat slabs a finite element model was created using ABAQUS. Figures 4.5, 4.6, and 4.7 show concrete failure in the slabs with and without channels and steel plates on the top, respectively. The geometry of the slabs, supports, and loads reflected the experiments. The numerical moment versus displacement curves of the slab with and without strengthening from above is presented in Figure 4.8. The model predicted that the channels would add 29% additional moment capacity relative to the baseline slab (14 ft.), and the plates would add

18% additional moment capacity relative to the baseline slab. The model was slightly conservative for the baseline slab and unconservative for the strengthened slab. Based on the favorable comparison between the models and experiments, the model parameters (element types, mesh sizes, material properties, boundary conditions, and load application) may be helpful for capturing the global response of baseline and strengthened slabs in future experiments. Note that the reinforcement bar yield stress in the finite element models was 60,000 psi. Agreement between the FE model and experiments suggests that the reinforcement in the test specimens may be in the range of 60,000 psi.

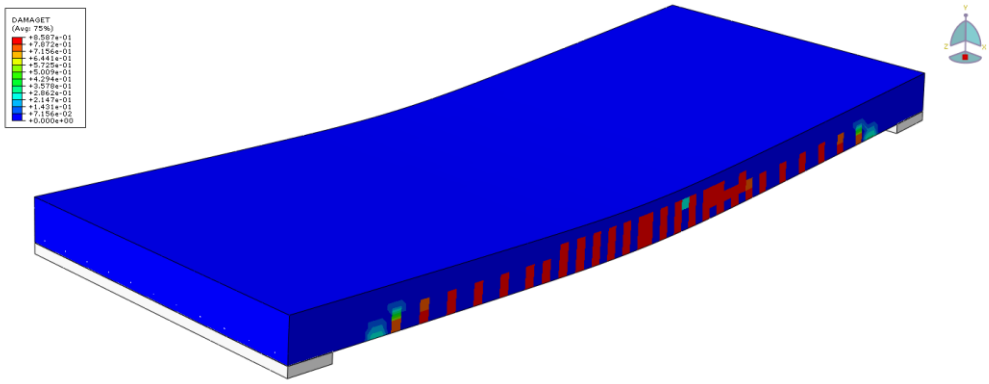

Figure 4.5 Finite element modeling of baseline flat slab.

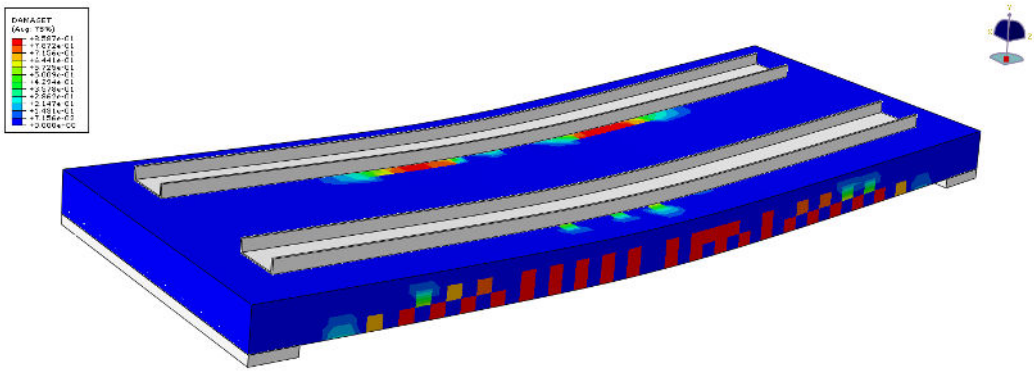

Figure 4.6 Finite element modeling of flat slab strengthened by steel channels.

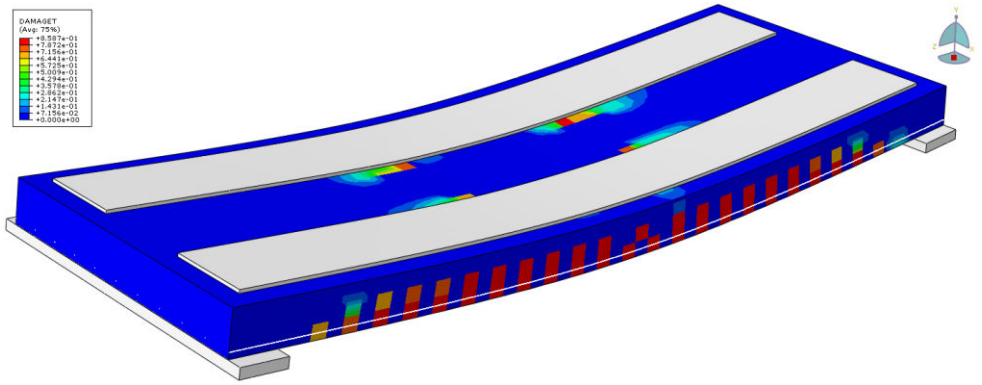

Figure 4.7 Finite element modeling of flat slab strengthened by steel plates.

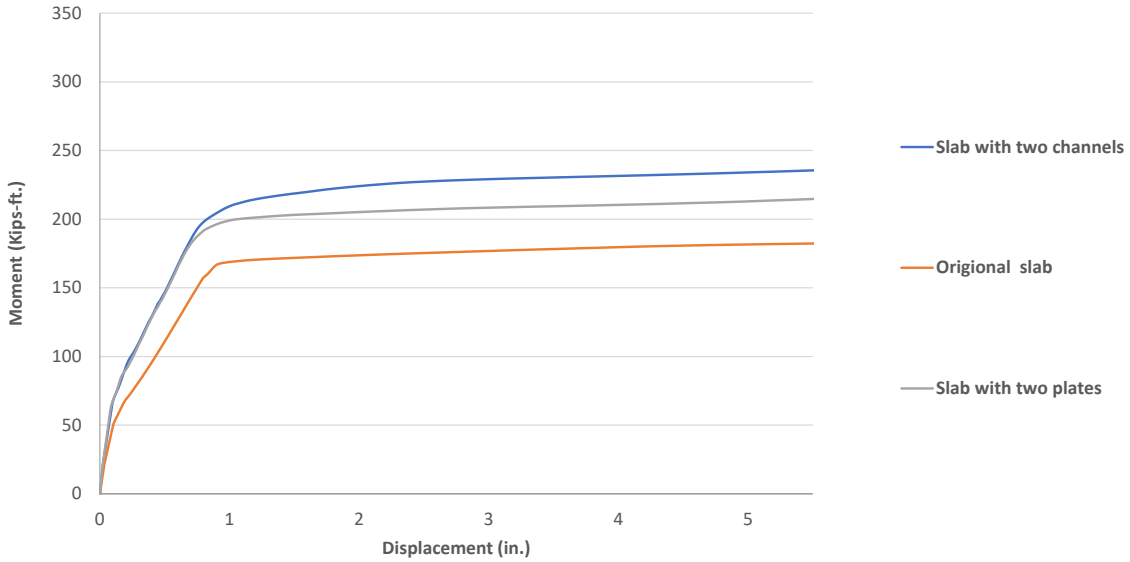

Figure 4.8 FE results: Moment versus displacement curves for strengthening from above

4.4 Results of NSM

Results of the NSM test are different than the other strengthening methods due to the different boundary conditions related to creating a continuous span from two slabs in series. The previous strengthening methods utilized the addition of steel to the cross section of the slab, whereas the NSM approach distributes moment to the negative moment region over the joint of the two slabs. As a result, the applied load required to achieve the total moment capacity has been increased. To compare with the other strengthening methods, the measured moment capacity for a single span (four-point test) was calculated by multiplying half of the measured applied load to the shear span.

Table 4.4 demonstrates the comparison of baseline specimen (Unstrengthened) and strengthened NSM specimen.

The failure mode of the NSM test also differed from that of all other strengthening approaches and the baseline specimens. Typical slab behavior at failure exhibited yielding of reinforcement and crushing of concrete at the slab surface at or near midspan. It also exhibited shear cracking in the shear span at the slab end farthest from the slab joint. Reasons for this phenomenon could be attributed to damage to the slab itself and increased shear forces due to the addition of NSM bars over the joint. Slab conditions post-failure can be observed in Figures 4.9 and 4.10.

Table 4.4 Comparison of baseline specimen and strengthened NSM specimen

	Measured Yield Load (kip)	Measured Failure Load (kip)	Measured Yield Moment (kip-ft)	Measured Moment capacity (kip-ft)	Measured Yield Moment/ Baseline Yield Moment	Measured Moment Capacity / Baseline Moment Capacity
Average of Baseline specimen (Unstrengthened)	64	78.5	169	208	N/A	N/A
Strengthened with NSM steel bars	76	97.0	201	257	1.19	1.23
*N/A refers to not applicable.						

Figure 4.9 Failure mode of NSM test

Figure 4.10 Debonding and cracking of grout

4.5 Performance of the drone inspection using deep learning models

The binary classification of cracks used a CNN model to detect the presence of cracks. The multi-class CNN model was developed to classify the cracks into separate damage zones to indicate the damage severity.

The input images were divided into two groups based on the presence of the crack. The 20,000 input images without cracks labelled as “Undamaged” and the 20,000 input images with cracks labelled as “Crack” were input into the CNN model. 70% of the images were used to train the model and 30% of the data were used to test the model. After the execution of the model, the CNN model was able to classify and assign the correct labels with an accuracy of 99.9% (Figure 4.9). Out of 6,000 images, 5,996 images were correctly classified as “Undamaged”. 5,992 images out of 6,000 images were correctly classified as “Crack”. A CNN model was developed for the detection of cracks in the images of concrete surfaces.

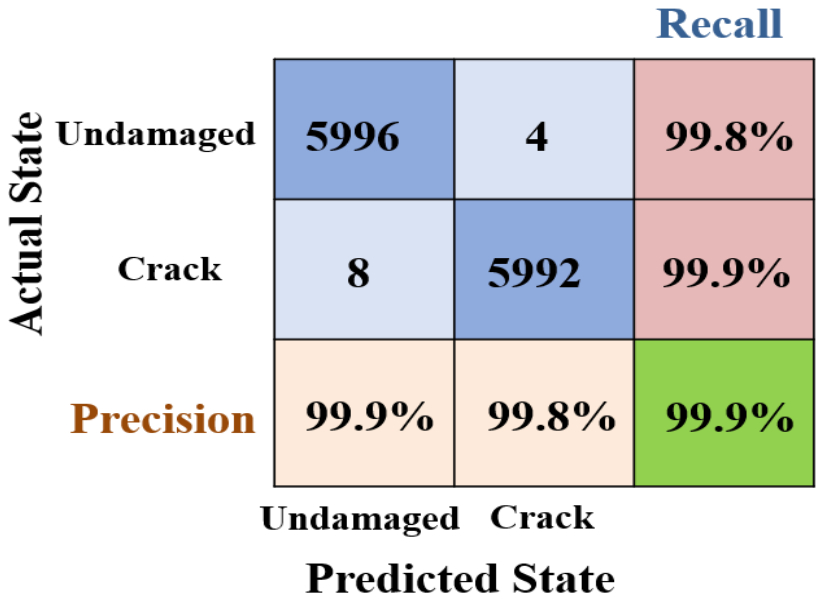

Figure 4.11 Confusion matrix for crack detection

The images with their respective labels based on the depth of the crack were input to the multi-class CNN model. The CNN model extracts the features and classifies the images to their respective zones. A total of 549 images generated in the image database were used for the classification. The image database was split to 70% and 30% for training and testing, respectively. In the confusion matrix, an accuracy of 87.9% was obtained in classifying the images based on the depth of the cracks (Figure 4.12). Out of 58 images in Zone 1, 53 images were correctly classified to Zone 1. Out of 58 images in Zone 2, 58 images were correctly classified to Zone 2. Out of 58 images in Zone 3, 42 images were correctly classified to Zone 3.

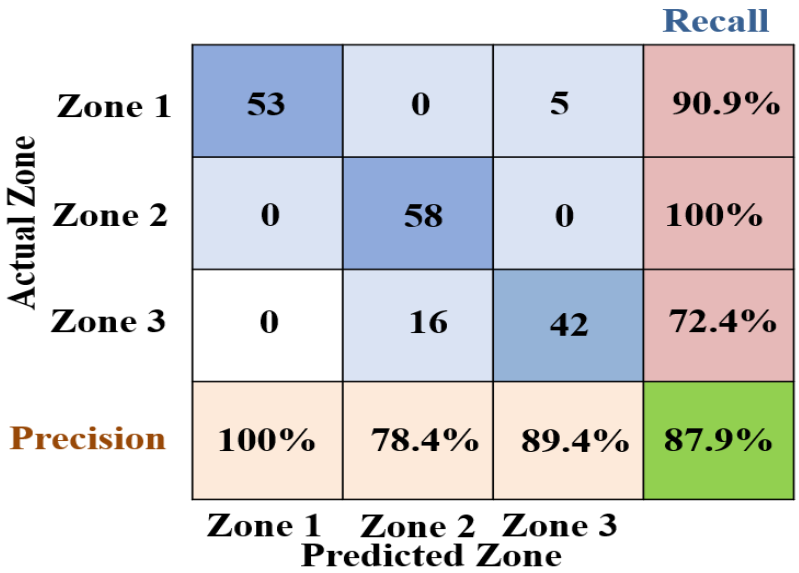

Figure 4.12 Confusion matrix for damage severity

4.6 Cost analysis of strengthening methods

When analyzing a bridge with a deficient load rating, the bridge engineer is faced with deciding from three alternatives: (1) replacing the existing bridge, (2) strengthening the existing bridge (which also includes selecting the "best" strengthening method from those available), or (3) leaving the existing bridge in its present state. Deciding among the three alternatives involves several factors, all of which must be carefully evaluated. The most effective method of selecting an alternative is accomplished by evaluating the economic advantages associated with each alternative. By attempting to quantify each alternative in terms of its economic value, the engineer can achieve a rational method of making comparisons among alternatives.

One of the goals of this project is to determine and evaluate the cost benefit of different strengthening approaches of flat slab bridges. This section proposes a method to estimate the costs of each strengthening approach in the field to compare the practicality of applying these methods. The strengthening techniques are divided into two types: strengthening the slab from above and strengthening the slab from the bottom, which will affect the cost estimate. Finally, the cost estimate method is presented in a case study of a bridge near Abbeville SC.

4.6.1 Case study: Abbeville bridge

The bridge is S-97 over Johnson Creek near Abbeville, SC. The bridge is simply supported with eight spans each 15 foot long. Each span consists of four interior and two exterior panels (flat slabs with 9.25 in. thickness) supported by a reinforced concrete pier cap and timber piles. The bridge is two lanes wide without shoulders or emergency lanes, and the overall bridge width is 27.5 ft. while the roadway width is 26 ft. Each lane consists of two interior panels, and the panels are spaced 5.5 ft apart while the piles are set apart by 5’ - 10.5”. The number of panels to be strengthened is 32, all the interior panels along the bridge. Figures 4.13 and 4.14 present a photograph of the bridge and a cross-section.

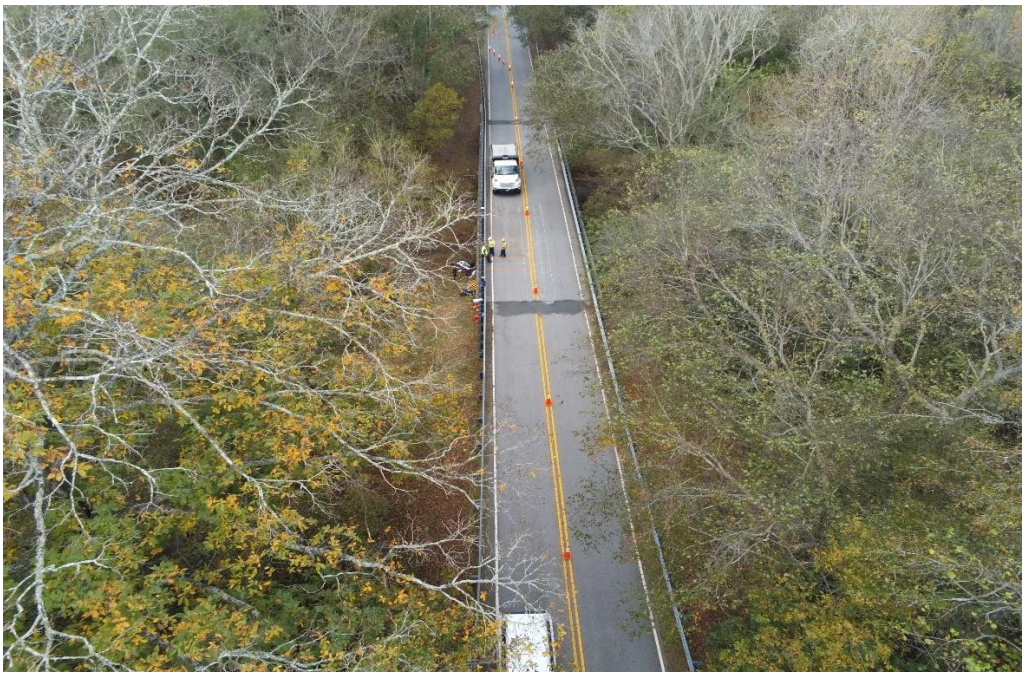

Figure 4.13 S-97 bridge (Abbeville bridge).

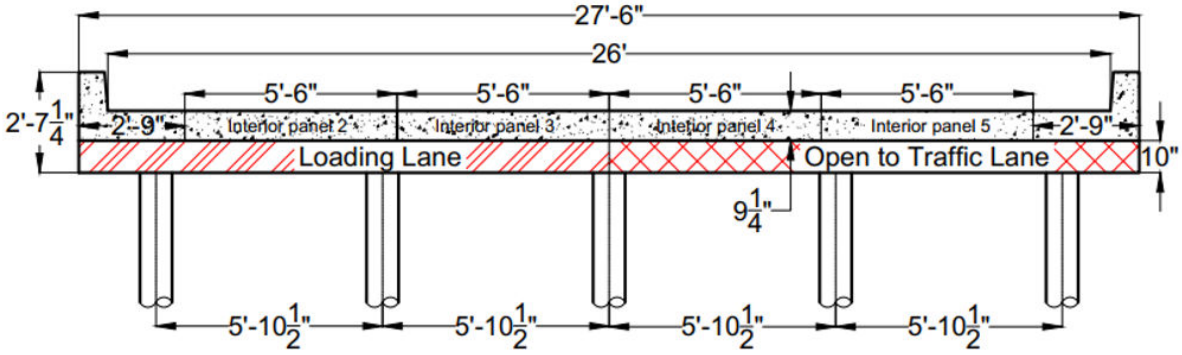

Figure 4.14 Cross Section of Abbeville bridge.

4.6.2 Factors that influence the cost

Five distinct factors will be considered for the cost estimate: materials, labor, lane closures, overlay layer, scaffolding and snooper truck. Hence, to estimate the cost for the several factors, some assumptions have been made:

1. Closing only one lane at a time to strengthen the bridge
2. One laborer per panel working at the same time
3. The number of scaffoldings is equal to the number of panels per lane
4. Two snooper trucks working at the same time

4.6.2.1 Materials cost

The principal material components of the strengthening methods include grout, epoxy, bolts, nuts, and steel. The materials cost was calculated based on the quantity needed in the laboratory tests and was converted into field needs. This cost estimate does not include the equipment used for drilling the holes. Tables 4.5 through 4.12 present the materials cost for the strengthening methods employed for the Abbeville Bridge.

Table 4.5 Materials cost for steel plates from below (Method 1) strengthening method

Steel Plates from below (Method 1)				
Items	Details	Quantity	Unit Cost	Subtotal
Grout	Sika 212	3200 lb	$/lb 0.20	$640
Steel	3” x 1/2” plates	4573 lb	$/lb 1.50	$6860
Nuts	5/8” A307	1536	$0.50	$768
Bolts	5/8” A307	768	$5.00	$3840
Total				$12,108

Table 4.6 Materials cost for steel plates from below (Method 2) strengthening method

Steel Plates from below (Method 2)				
Items	Details	Quantity	Unit Cost ($)	Subtotal ($)
Grout	Sika 212	1600 lb	$/lb 0.20	$320
Steel	3” x 1/2” plates	4573 lb	$/lb 1.50	$6860
Nuts	5/8” Grade 8	768	$0.50	$384
Bolts	5/8” Grade 8	384	$6.00	$2304
Total				$9868

Table 4.7 Materials cost for steel plates from below (Method 3) strengthening method

Steel Plates from below (Method 3)				
Items	Details	Quantity	Unit Cost ($)	Subtotal ($)
Grout	Sika 212	800 lb	$/lb 0.20	$160
Steel	3-3/4” x 1/2” plates	2858 lb	$/lb 1.50	$4287
Nuts	3/4” Grade 8	384	$0.50	$192
Bolts	3/4” Grade 8	192	$6.00	$1152
Total				$5791

Table 4.8 Materials cost for steel plates from below (Method 4) strengthening method

Steel Plates from below (Method 4)				
Items	Details	Quantity	Unit Cost ($)	Subtotal ($)
Grout	Sika 212	550 lb	$/lb 0.20	$110
Steel	2-1/2” x 1/2” plates	1906 lb	$/lb 1.50	$2860
Nuts	3/4” Grade 8	256	$0.50	$128
Bolts	3/4” Grade 8	128	$6.00	$768
Total				$3866

Table 4.9 Materials cost for steel channels from above strengthening method

Steel Channels from Above				
Items	Details	Quantity	Unit Cost ($)	Subtotal ($)
Epoxy	DeWalt Pure110+	32	$40.00	$1280
Steel	A36 C10*15.3	13,171 lb	$/lb 1.50	$19,756
Nuts	Steel Hex Nut Grade 5, 7/8”	640	$0.35	$224
Bolts	5/8” Grade B7 threaded rod	640	$3.00	$1920
Total				$23,180

Table 4.10 Materials cost for steel plates from above strengthening method

Steel Plates from Above				
Items	Details	Quantity	Unit Cost ($)	Subtotal ($)
Epoxy	DeWalt Pure110+	64	$40.00	$2560
Steel	A572 GR 70 5/8”x16”x168”	24,391 lb	$/lb 1.50	$36,587
Nuts	Steel Hex Nut Grade 5, 7/8”	640	$0.35	$224
Bolts	5/8” Grade B7 threaded rod	640	$3.00	$1920
Total				$41,291

Table 4.11 Materials cost for NSM steel bars from above strengthening method

NSM Steel Bars from Above				
Items	Details	Quantity	Unit Cost ($)	Subtotal ($)
Grout	Sakrete Non-Shrink	3200 lb	$/lb 0.4	$1,280
Steel	#6 bars Grade 60, 10’ long	192	$12	$2,304
Grooves	chipping 6 grooves in two adjacent longitudinal slabs	16	$1,281	20,496
Total				$24,080

Table 4.12 Materials cost for external post tensioning from below strengthening method

External Post-Tensioning from bottom				
Items	Details	Quantity	Unit Cost ($)	Subtotal ($)
Rods	5/8" Dywidag Threaded Rods GR 160 cut @ 12'-6"	96	$63.90	$6,134
Nuts	Steel Hex Nut Grade 5	768	$0.93	$714
	5/8" Dywidag 5/8" Hex Nut	256	$30.84	$7,895
Bolts	7/8" threaded rod, 4" long	96	$ 61.64	$5,917
Steel	6"x 6" outside size, 1" thickness, 3' long, 90-degree angle	23,520 lb	$/lb 1.50	$38,886
	12" x 36" x 0.5", plate	1962 lb	$/lb 1.50	
	4" x 4"x 0.5", plate	442 lb	$/lb 1.50	
Total				$59,546

4.6.2.2 Labor cost

The cost estimation for labor-hours is set at $20/hour as per the South Carolina prevailing wage. The working hours were calculated based on the drilling of the slabs and the installation of steel. The drilling time for a hole for the strengthening from above methods is 10 min, while strengthening from the bottom methods is 40 min based on the laboratory tests. Table 4.13 shows the labor cost for the strengthening methods employed for the Abbeville Bridge.

Table 4.13 Labor cost

Strengthening Method	Labor hours	No. of labors	Labor Cost per lane	Total Labor Cost
Steel Plates from below (Method 1)	16	16	$5120	$10,240
Steel Plates from below (Method 2)	8	16	$2560	$5120
Steel Plates from below (Method 3)	4	16	$1280	$2560
Steel Plates from below (Method 4)	3	16	$960	$1920
Steel Channels from Above	3.5	16	$1120	$2240
Steel Plates from Above	7.5	16	$2400	$4800
NSM Steel Bars from Above	5.5	16	$1760	$3520
External Post-Tensioning from bottom	2	16	$640	$1280

4.6.2.3 Lane closure cost

The cost estimation for lane closure cost is set at $200/hr as it requires equipment and crews to man signage and direct traffic. The time of the installation of the overlayer is the sum of the time required to install the overlay layer and 24 hours required before opening the lane. Several factors are considered while calculating the time required for the lane closure of Abbeville Bridge, presented in Table 4.14.

Table 4.14 Lane closure cost

Strengthening Method	Drilling and Installation (hr)	Curing time for Epoxy/Grout (hr)	Installation of the overlay layer (hr)	Time for the lane closure (hr)	Cost of one lane closure	Total Cost of lanes closure
Steel Plates from below (Method 1)	16.0	48	--	64.0	$12,800	$25,600
Steel Plates from below (Method 2)	8.0	48	--	56.0	$11,200	$22,400
Steel Plates from below (Method 3)	4.0	48	--	52.0	$10,400	$20,800
Steel Plates from below (Method 4)	3.0	48	--	51.0	$10,200	$20,400
Steel Channels from Above	3.5	8	32	43.5	$8700	$17,400
Steel Plates from Above	7.5	8	32	47.5	$9500	$19,000
NSM Steel Bars from Above	5.5	8	32	45.5	$9,100	$18,200
External Post-Tensioning from bottom	2.0	8	32	42.0	$8400	$16,800

4.6.2.4 Overlay layer cost

Local companies were contacted to calculate the price of installing a 3” overlay layer. Two cases were considered regarding the existence of the asphalt layer. For an existing asphalt layer, the cost included the removal of the existing asphalt layer and installing a new one; however, the area removed was just sufficient to install the strengthening materials. While for the case with no existing asphalt layer, the cost was calculated based on installing an asphalt layer for the whole bridge area. Based on the estimated costs provided by S&J Asphalt Paving LLC, the installation

of the overlay layer would cost $8215, and the removal of the existing asphalt layer estimated for the whole bridge area would cost $3931. The cost includes materials delivered, labor for installation, equipment, and fuel. Table 4.15 shows the overlay layer cost for the Abbeville bridge.

Table 4.15 Overlay layer cost

Strengthening Method	Cost of Overlay layer (No Existing Asphalt)	Cost of Overlay Layer (Existing Asphalt)
Steel Channels from Above	$8215	$5880
Steel Plates from Above	$8215	$7358
NSM Steel Bars from Above	$8215	$6330
External Post-Tensioning from bottom	$8215	$3731

4.6.2.5 Scaffolding and snooper truck

Local companies were contacted to calculate the price of renting scaffolding and snooper trucks. The scaffolding tower is 10 ft long, 5 ft width, and 10 or 15 ft in height. According to these dimensions, one tower will only cover one slab panel. Sunbelt Rentals provided a rough cost estimate for comparison purposes; one scaffolding tower would cost $3272. This cost includes equipment, erection, dismantlement, and freight.

On the other hand, McClain & Co. Inc., provided a quote for the snooper truck that would cost $3811 per day. Again, this cost includes equipment, driver and basket operator, mobilization, and tolls. The additional cost of lane closure is based on 8 hour/day for 4 days, which is the time the snooper truck is required to install the strengthening system. Table 4.16 presents the scaffolding and Snooper truck cost for the Abbeville Bridge site.

Table 4.16 Scaffolding and snooper truck cost

Strengthening Method	Cost of Scaffolding	Cost of Snooper Truck Rental	Additional Cost of Lane closure and Labor	Total Cost of Snooper Truck
Steel Plates from below (Method 1)	$86,464	$30,492	$6400	$36,892
Steel Plates from below (Method 2)	$86,464	$30,492	$6400	$36,892
Steel Plates from below (Method 3)	$86,464	$30,492	$6400	$36,892
Steel Plates from below (Method 4)	$86,464	$30,492	$6400	$36,892
External Post-Tensioning from bottom	$86,464	$30,492	$6400	$36,892

4.6.3 Cost analysis results

Tables 4.17 through 4.19 present the total cost and the moment capacity increase (%) for the strengthening methods. First, the measured moment capacity increase (%) was calculated based on the measured moment capacity for the strengthened slab with respect to average measured baseline (Unstrengthened). Second, the measured moment capacity increase (%) was calculated based on the measured moment capacity for the strengthened slab with respect to calculated baseline (Unstrengthened). Figures 4.15 and 4.16 show the total cost versus the moment capacity increase (%) for each strengthening method.

Table 4.17 Total Cost and Moment Capacity Increase (%) for strengthening from above methods

Strengthening Method	Total Cost (No Existing Asphalt)	Total Cost (Existing Asphalt)	Measured Moment Capacity Increase (%) with respect measured baseline	Measured Moment Capacity Increase (%) with respect calculated baseline
Steel Channels from Above	$51,036	$48,700	12.0	89.4
Steel Plates from Above	$73,306	$72,449	4.3	76.4
NSM Steel bars from Above	$54,015	$52,130	23.0	108.9

Table 4.18 Total Cost and Moment Capacity Increase (%) for strengthening from below methods

Strengthening Method	Total Cost (Scaffolding)	Total Cost (Snooper Truck)	Measured Moment Capacity Increase (%) with respect measured baseline	Measured Moment Capacity Increase (%) with respect calculated baseline
Steel Plates from below (Method 1)	$134,412	$84,840	21.2	104.9
Steel Plates from below (Method 2)	$123,852	$74,280	40.9	138.2
Steel Plates from below (Method 3)	$115,615	$66,043	28.8	117.9
Steel Plates from below (Method 4)	112,650	$63,078	13.0	91.1

Table 4.19 Total Cost and Moment Capacity Increase (%) for external post tensioning from below

Strengthening Method	Total Cost (No Existing Asphalt/ Snooper)	Total Cost (Existing Asphalt/ Snooper)	Measured Moment Capacity Increase (%) with respect measured baseline	Measured Moment Capacity Increase (%) with respect calculated baseline
External Post-Tensioning from bottom	$122,733	$118,250	42.3	140.7

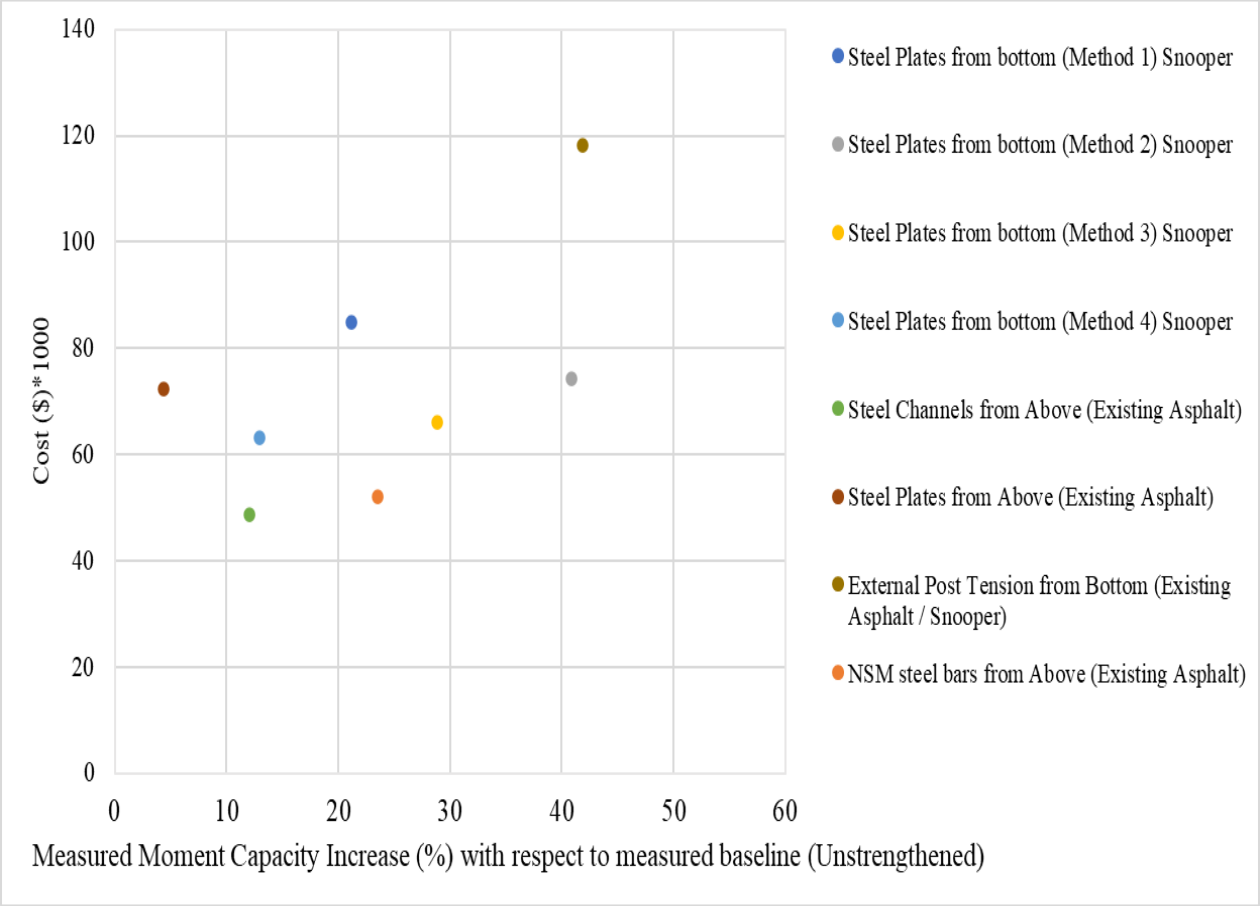

Figure 4.15 Total Cost vs. Measured Moment Capacity Increase (%) with respect to measured baseline (Unstrengthened).

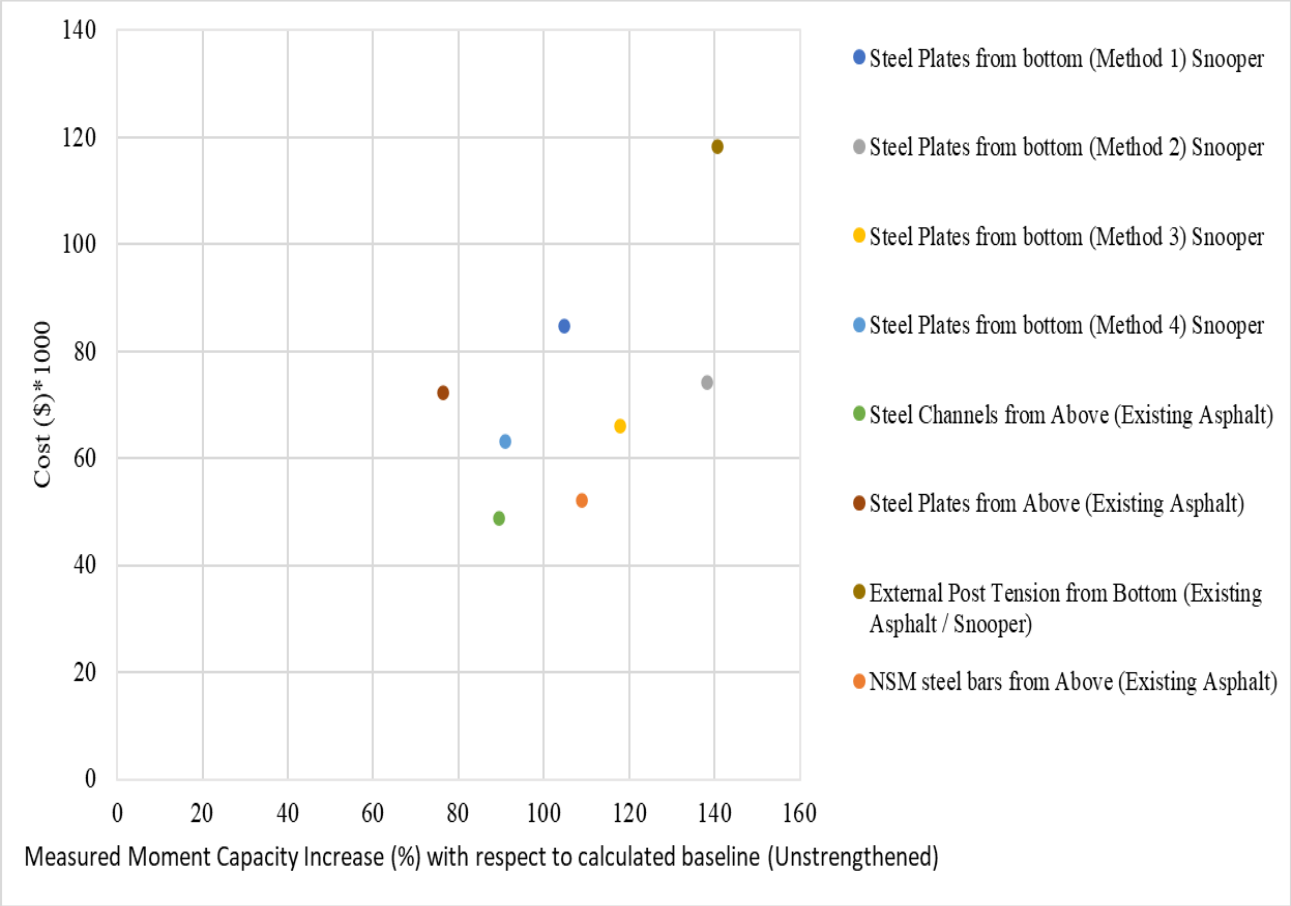

Figure 4.16 Total cost vs Measured Moment Capacity Increase (%) with respect to calculated baseline (Unstrengthened).

CHAPTER 5: DISCUSSION

Specific performance issues associated with flat slabs have been studied and documented in this report. Laboratory investigations of both flat slabs and different strengthening approaches have been presented in the preceding chapters.

Reinforced concrete flat slab sections are commonly used in bridges by the South Carolina Department of Transportation. Many flat slab bridges were originally designed to resist H10 or H15 truck loading. Strengthening of flat slab bridges from below is challenging due to access issues and the need to work overhead. To minimize these challenges while still achieving a net benefit, an approach of strengthening from above was pursued in addition to strengthening from below. The approaches described in this report have to do with the bolting of steel shapes to the top and bottom surface of the slab section, external post tensioning, and mounting near surface bars to the top of the slab surface. The load-deflection response can be characterized by three stages: 1) pre-cracking with a linear load-deflection response, 2) an almost linear cracked stage up to yielding of the embedded reinforcement, and 3) a significant post-yielding phase up to the maximum load. The average of the baseline yield loads was 62 kips and 65 kips for 14' and 15' slabs, respectively. For the strengthened slab with channels this was 62 kips, for the strengthened slab with plates on the top 70 kips. For the strengthened slabs with plates on the bottom with 24 holes the value was 95 kips, with 16 holes was 72 kips, with 6 holes was 65 kips and with four holes was 58 kips, respectively. The test with post-tensioning from the bottom resulted in a yield load of 83 kips, while the NSM tested exhibited a yield load of 76 kips. Concrete crushing was observed in both the baseline and strengthened slabs.

The strengthening from the bottom with steel plate with 16 holes increases the flexural strength up to 41%. The total moment for the strengthened slab with steel channels from above was a 12% increase compared to the average moment capacity of the baseline slabs with bearing boundary conditions. The slab with steel plates from above increased the moment capacity by around 4% compared to the average moment capacity of the baseline slabs. The slab with external post tensioning increased the moment capacity by around 42% compared with the average moment capacity of the baseline slabs. The near surface mounted bars also increased peak load capacity by 23% compared to the average peak load capacity of the baseline slabs.

According to the cost analysis on the different strengthening approaches, the strengthening method proposed based on the desired moment capacity increase is as follows for the Abbeville bridge:

It shows that the cheapest method is strengthening with steel channels from above, up to a target of 10% moment capacity increase. While, up to a target of 20% moment capacity increase, strengthening with NSM steel bars from above is recommended. In addition, up to a target of 29% moment increase, strengthening with steel plates from below (Method 3) with Snooper truck is recommended. Furthermore, up to a target of 39 % moment capacity increase, strengthening with steel plates from below (Method 2) with Snooper truck is recommended, and up to a target of 42% moment capacity increase, strengthening with external post-tensioning from below with Snooper truck is recommended.

SCDOT data shows that most flat slab bridge rating factors fall within the range 0.65-.075. Specifically, 1003 out of 1450 bridges fall within this rating factor range. This means that the demand exceeds the capacity by 25%-35% for most slabs that require strengthening. Therefore, the most ideal target strength increase should be in the ranges of 25%-35% to satisfy most bridge

cases in the state. Out of the methods already tested, this range corresponds to NSM bars (23%) and steel plates on the bottom (Method 3) (29%), of which NSM bars is the cheaper option by $10,000 based on the Abbeville bridge case study. Even though many factors can affect which method is most suitable for individual bridges, the data suggests that NSM bars would be the cheapest alternative for most flat slab bridges in South Carolina.

The baseline (unstrengthened) 14' and 15' flat slabs exhibited capacities that overperformed theoretical capacities based on material properties and geometry gathered from SCDOT documents and records. Moreover, potential factors for the inflated capacities were identified and are listed as such. First, there may be differences in actual versus theoretical effective depth of reinforcement due to varying clear cover measurements at the bottom of the slabs. Second, it is possible that existing steel reinforcement exhibited higher stresses after yield, where no idealized yield plateau has occurred, due to strain hardening. Lastly, actual compressive strength of concrete varies from specimen to specimen effecting experimental results but was not considered in the theoretical calculations. The tested cores and rebars had higher values for the compressive strength of the concrete and tensile strength of the rebars than the theoretical values from SCDOT documents and records as shown in Tables 3.1 and 3.2. A combination of these factors can lead to the higher measured moment capacity attained. Sensitivity analysis was performed to assess the impact of changing the effective depth of reinforcement (d), the compressive strength of concrete (f_c'), or the yield strength of the rebars (f_y) on the moment capacity of the slabs. Figure 5.1 presents the sensitivity analysis for these three variables on the moment capacity. Varying the effective depth yielded the highest impact on the increase of the moment capacity. While increasing the compressive strength of concrete had the least effect on the increase of the moment capacity.

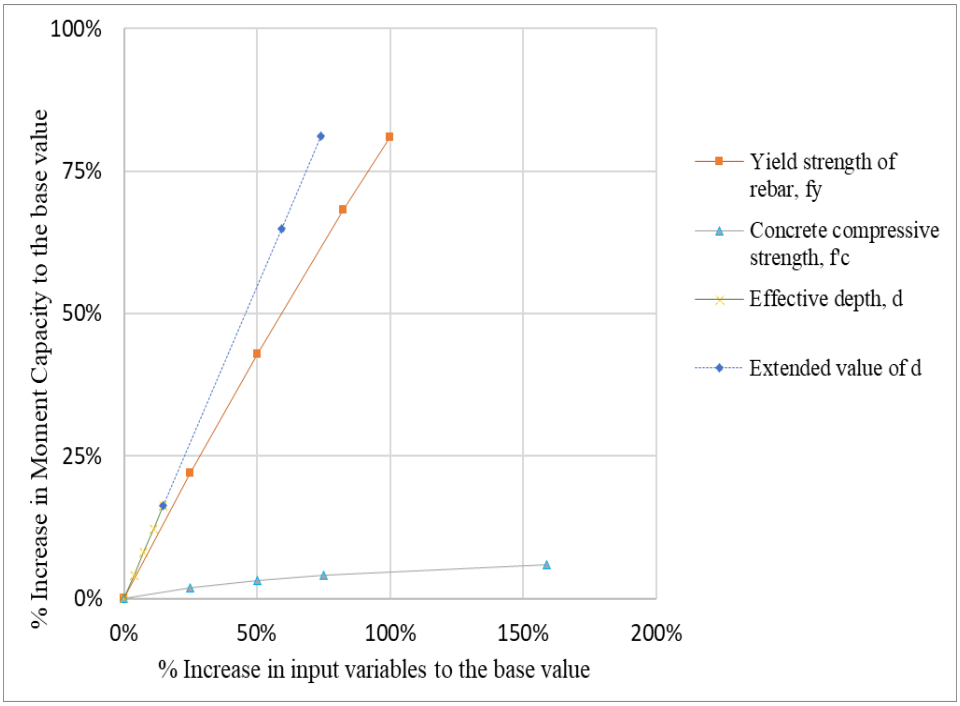

* The base values were 4000 psi, 40000 psi, and 6.75 in. for f_c' , f_y , and d, respectively.

Figure 5.1 Sensitivity analysis

Two CNN models were developed in the study for automated inspection of the bridge. A CNN model was developed in the study to detect the presence of the cracks in the images of the concrete surfaces. An accuracy of 99.9% was obtained for the model. This model can be used to inspect the images taken from the bridge site to detect cracks. A multiclass CNN model was developed which can determine the severity of the cracks based on the crack depth. An accuracy of 87.9% was obtained for the model. This model can be used to determine the damage severity of the cracks in the images taken from the bridge site.

CHAPTER 6: CONCLUSIONS AND RECOMMENDATIONS

This report considers cost-effective design and strengthening strategies to improve the performance of flat slab superstructures. These components were selected through consultation with the SCDOT as they are common throughout the bridge inventory and addressing performance issues will have a broad impact. Challenges associated with these components include a) structural capacities based on lower truck loads than are used today, and b) ages that are approaching or exceeding expected lifespan along with associated deterioration. The work described in this report is part of a larger effort to extend the useful life of bridges in South Carolina.

Specific goals addressed include:

- Benchmarking the flexural strength of precast concrete flat slabs.
- Evaluating a flat slab strengthening method using steel sections bolted to the top of the slab and steel plates on the top of the slab.
- Evaluating a flat slab strengthening method using steel plates bolted to the bottom of the slab.
- Evaluating a flat slab strengthening method using external post tensioning at the bottom of the slab.
- Evaluating a flat slab strengthening method using near-surface mounted bars on top of the slab joint.
- Evaluating traditional and numerical models of flat slabs.
- Develop methods for automated drone inspection of the bridges
- Cost-effective analysis on different strengthening approaches

6.1 Conclusions

Conclusions regarding the goals are summarized below.

Benchmarking the flexural strength of precast concrete flat slabs. Baseline flat slab behavior was established in four-point bending regarding moment capacity and modes of failure. On average, baseline measured yield and failure moments were higher than calculated yield and failure moments based on material properties and geometry indicated in the construction documents. The slabs performed better than anticipated, with 15' specimens outperforming 14' specimens when comparing measured over-calculated moment results as shown in Figures 6.1 and 6.2.

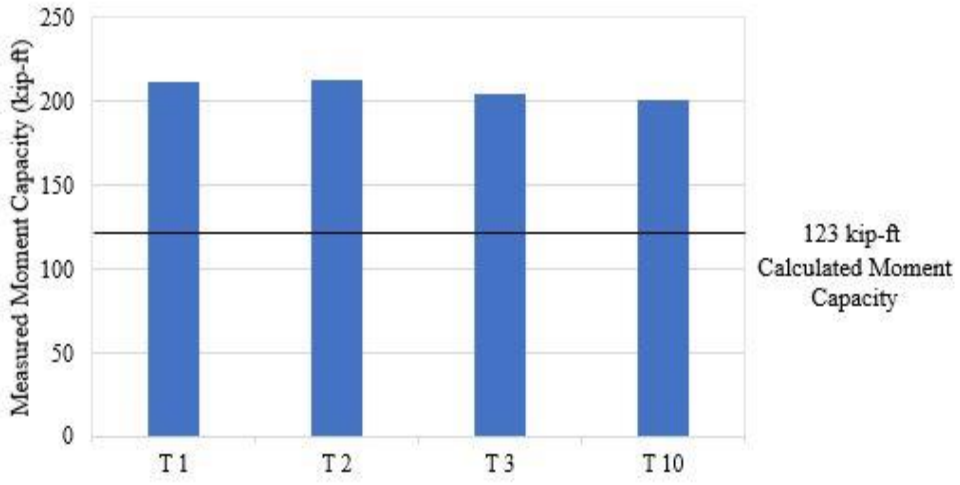

* The average measured moment capacity for the 14' long slabs is 208 kip-ft.

Figure 6.1 Unstrengthened Slab Results (14' ft long).

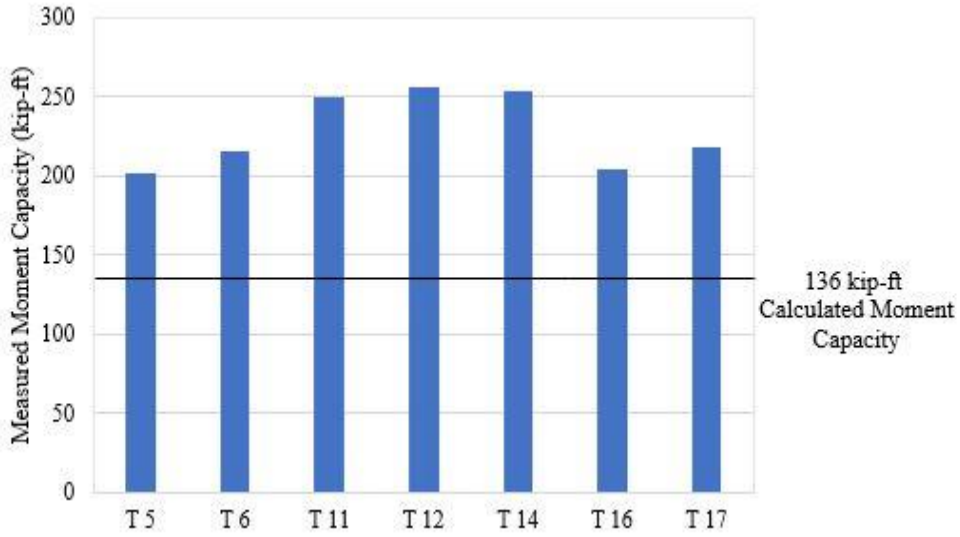

* The average measured moment capacity for the 15' long slabs is 228 kip-ft.

* The average 15’ long slab moment capacity does not include the result from test 4 due to inconsistencies from the roller bearing support condition.

Figure 6.2 Unstrengthened Slab Results (15' ft long).

Evaluating increases in capacity from flat slab strengthening methods. As shown in Figure 6.3, the lowest overall strength increase was achieved by mounting steel plates to the surface of the slabs. This exhibited a moment capacity increase of 4% with respect to measured baseline. The highest overall strength increase was achieved by post-tensioning the slab with mechanically torqued tension rods on the bottom of the slab. This demonstrated a moment capacity increase of 42% with respect to measured baseline. In general, strengthening from below will increase capacity more than strengthening from above (excluding NSM).

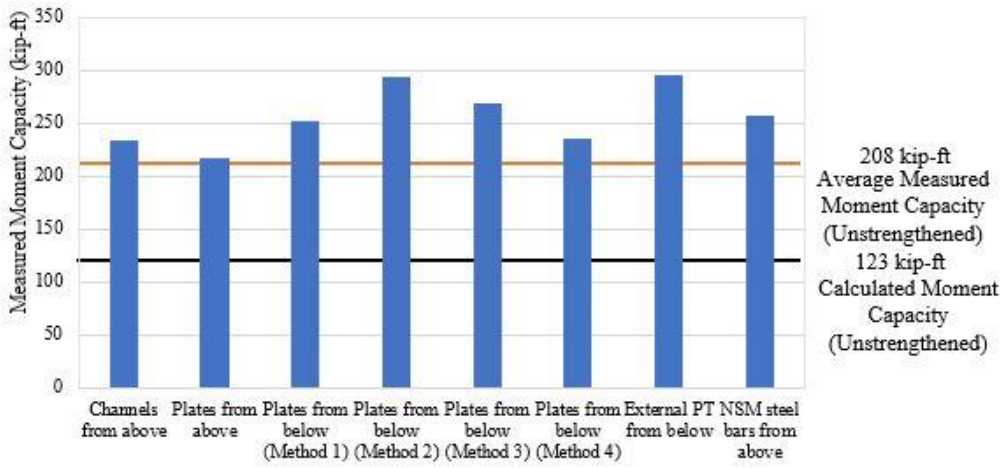

* The average measured moment capacity for the 14' long slabs is 208 kip-ft.

* The calculated moment capacity for the 14’ long slabs determined by using conventional reinforced concrete strength design concepts with specified concrete and steel material properties is 123 kip-ft.

Figure 6.3 Strengthened Slab Results (14' ft long).

Evaluating cost of flat slab strengthening methods from the top and from the bottom. Cost-benefit analysis shows that overall material cost is more expensive for strengthening from above. However, due to constructability concerns and special methods of access, it is more expensive overall to strengthen from the bottom than it is from the top. The two cheapest methods were strengthening from above with NSM steel bars and Channels. While the most expensive methods were strengthening from below with external post tensioning and steel plates (Method 1).

Determining appropriate methods of strengthening for a target moment capacity increase. To determine the appropriate method of strengthening, a judgment should be made based on the cost and the moment capacity demand. If there are no restrictions to access the bridge from the top or bottom, the cheapest method to satisfy the moment capacity demand should be chosen. Up to a target of 10% moment capacity increase, strengthening with steel channels from above is the cheapest method. With a target of 10 to 20% moment capacity increase, the cheapest strengthening method is NSM steel bars from above. With a target of 20 to 30% moment capacity increase, strengthening with steel plates from below (Method 3) is the cheapest method. In addition, strengthening with steel channels from below (Method 2) is the cheapest method for a target of 30 to 45% moment capacity increase.

Determining best method of strengthening for South Carolina. It is challenging to predict the unique factors that could affect the applicability of certain strengthening methods from the bridge to bridge. SCDOT data suggests that 1003 out of 1450 bridges in South Carolina require a strength increase of 25%-35%. Based on this requirement, the cheapest alternative to achieve this strength range is the NSM bars from above, also making it the best method of selection for most bridges in the state.

6.2 Recommendations and future work

The following recommendations are provided for strengthening flat slabs:

1. Investigation of different strengthening approaches, potentially including fiber reinforced polymers, and similar material and structural systems should be considered. Supplemental concrete deck toppings could likewise be considered.
2. Comparisons on the different additional strengthening approaches are recommended in terms of material cost, labor time, traffic closure cost, and ease of application in the field to arrive at the other promising strengthening approaches.
3. Further trials of drone inspection, data analysis, and asset management software should be explored to streamline the bridge inspection process and reduce costs while reducing safety risks.

REFERENCES

AASHTO (2017). Bridge design specifications. American Association of State Highway and Transportation Officials, AASHTO: Washington, DC, USA.

Abdel-Qader, I., Abudayyeh, O., & Kelly, M. E. (2003). Analysis of edge-detection techniques for crack identification in bridges. Journal of Computing in Civil Engineering, 17(4), 255-263.

Cha, Y. J., Choi, W., & Büyüköztürk, O. (2017). Deep learning-based crack damage detection using convolutional neural networks. Computer-Aided Civil and Infrastructure Engineering, 32(5), 361-378.

DYWIDAG threadbars - Technical Data [Metric Units].(2014). www.dsicanada.ca.https://buyandsell.gc.ca/cds/public/2017/10/16/5d2ac19b9441fc888aef6bbe68a72210/f1571-175051_drawing-dywidag_threadbars.pdf.

Fathelbab, F. A., Ramadan, M. S., & Al-Tantawy, A. (2014). Strengthening of RC bridge slabs using CFRP sheets. Alexandria Engineering Journal, 53(4), 843-854.

Gao, D., Fang, D., You, P., Chen, G., & Tang, J. (2020). Flexural behavior of reinforced concrete one-way slabs strengthened via external post-tensioned FRP tendons. Engineering Structures, 216, 110718.

Kim, H., Lee, J., Ahn, E., Cho, S., Shin, M., & Sim, S. H. (2017). Concrete crack identification using a UAV incorporating hybrid image processing. Sensors, 17(9), 2052.

Lee, S. H., Shin, K. J., & Lee, H. D. (2018). Post-tensioning steel rod system for flexural strengthening in damaged reinforced concrete (RC) beams. Applied Sciences, 8(10), 1763.

Lei, B., Wang, N., Xu, P., & Song, G. (2018). New crack detection method for bridge inspection using UAV incorporating image processing. Journal of Aerospace Engineering, 31(5), 04018058.

Metni, N., & Hamel, T. (2007). A UAV for bridge inspection: Visual surveying control law with orientation limits. Automation in construction, 17(1), 3-10.

Moon, H. G., & Kim, J. H. (2011). Intelligent crack detecting algorithm on the concrete crack image using neural network. Proceedings of the 28th ISARC, 1461-1467.

Moon, J., Reda Taha, M. M., & Kim, J. J. (2017). Flexural strengthening of RC slabs using a hybrid FRP-UHPC system including shear connector. Advances in Materials Science and Engineering, 2017.

Petrou, M. F., Parler, D., Harries, K. A., & Rizos, D. C. (2008). Strengthening of reinforced concrete bridge decks using carbon fiber-reinforced polymer composite materials. Journal of Bridge Engineering, 13(5), 455-467.

S&J Asphalt Paving LLC , 605 Battleground Rd. Chesnee, SC, USA

Savino, P., & Tondolo, F. (2021). Automated classification of civil structure defects based on convolutional neural network. Frontiers of Structural and Civil Engineering, 15(2), 305-317.

Sunbelt Rentals, 3535 N Graham st. Charlotte, NC, USA

Wibowo, H., & Sritharan, S. (2018). Use of ultra-high-performance concrete for bridge deck overlays (No. IHRB Project TR-683).

Xu, H., Su, X., Wang, Y., Cai, H., Cui, K., & Chen, X. (2019). Automatic bridge crack detection using a convolutional neural network. Applied Sciences, 9(14), 2867.

Yuan, F., Chen, M., & Pan, J. (2020). Flexural strengthening of reinforced concrete beams with high-strength steel wire and engineered cementitious composites. Construction and Building Materials, 254, 119284.

Zhu, J., & Song, J. (2020). An intelligent classification model for surface defects on cement concrete bridges. Applied Sciences, 10(3), 972.

Zhu, J., Zhang, C., Qi, H., & Lu, Z. (2020). Vision-based defects detection for bridges using transfer learning and convolutional neural networks. Structure and Infrastructure Engineering, 16(7), 1037-1049.

Zhu, Z., German, S., & Brilakis, I. (2011). Visual retrieval of concrete crack properties for automated post-earthquake structural safety evaluation. Automation in Construction, 20(7), 874-883.

APPENDIX A

Table A.1 Tensile strength of 6 rebar specimens in precast concrete slabs tested per ASTM E8

Specimen	Ultimate Tensile Strength (ksi)	0.2% Offset Yield Strength (ksi)	Yield point (ksi)	Elongation in 4D (%)	Reduction of Area (%)
C1*	74.5	43.6	47.1	31	57
C2*	92.5	53.0	56.0	31	49
C5*	74.0	44.1	46.5	32	57
P1**	74.5	43.8	50.0	32	58
P2**	75.0	43.8	46.5	30	56
P4**	75.0	44.7	48.2	30	59

**Specimens were taken from Test No. 7 (the flat slab with two C channels on the top).*

*** Specimens were taken from Test No. 8 (the flat slab with two steel plates on the top).*

Table A.2 Precast concrete slab compressive strength form core tested at USC per ASTM C 109

Test	Specimen	f_c' (psi)	Test	Specimen	f_c' (psi)	Test	Specimen	f_c' (psi)
10	1	5935	15	4	6823	16	4	6162
10	2	9642	7	1	8401	8	1	10275
10	3	9065	7	2	6133	8	2	8641
10	4	11120	7	3	4628	8	3	5723
12	1	5075	14	1	5790	*	1	5611
12	2	7126	14	2	5415	*	2	5706
12	3	7554	14	3	7588	*	3	6011
12	4	9554	14	4	8821	**	1	6469
17	1	8348	11	1	8304	**	2	6090
17	2	3960	11	2	10832	**	3	5740
17	3	9188	11	3	7742	**	4	6349
17	4	4345	11	4	8721	**	5	6950
15	1	8363	16	1	9581	**	6	7749
15	2	10016	16	2	7426			
15	3	7154	16	3	8115			

** and ** Specimens were taken from slabs that were not tested for the moment capacity.*